Published in final edited form as:

Cell. 2017 May 18; 169(5): 824–835.e14. doi:10.1016/j.cell.2017.05.003.

The U6 snRNA m^{6}A methyltransferase METTL16 regulates SAM synthetase intron retention

Kathryn E. Pendleton[1], **Beibei Chen**[2], **Kuanqing Liu**[3], **Olga V. Hunter**[1], **Yang Xie**[2], **Benjamin P. Tu**[3], and **Nicholas K. Conrad**[1,*]

[1]Department of Microbiology, UT Southwestern Medical Center, Dallas TX 75390

[2]Department of Clinical Sciences, UT Southwestern Medical Center, Dallas TX 75390

[3]Department of Biochemistry, UT Southwestern Medical Center, Dallas TX 75390

SUMMARY

Maintenance of proper levels of the methyl donor S-adenosylmethionine (SAM) is critical for a wide variety of biological processes. We demonstrate that the N^6-adenosine methyltransferase METTL16 regulates expression of human MAT2A, which encodes the SAM synthetase expressed in most cells. Upon SAM depletion by methionine starvation, cells induce MAT2A expression by enhanced splicing of a retained intron. Induction requires METTL16 and its methylation substrate, a vertebrate conserved hairpin (hp1) in the MAT2A 3′ UTR. Increasing METTL16 occupancy on the MAT2A 3′ UTR is sufficient to induce efficient splicing. We propose that under SAM-limiting conditions, METTL16 occupancy on hp1 increases due to inefficient enzymatic turnover, which promotes MAT2A splicing. We further show that METTL16 is the long-unknown methyltransferase for the U6 spliceosomal snRNA. These observations suggest that the conserved U6 snRNA methyltransferase evolved an additional function in vertebrates to regulate SAM homeostasis.

Graphical abstract

* Corresponding Author and Lead Contact: Nicholas.conrad@utsouthwestern.edu.

AUTHOR CONTRIBUTIONS

Conceptualization, N.K.C. and K.E.P.; Methodology, K.E.P., B.C., K.L., O.V.H., B.P.T., N.K.C.; Investigation, K.E.P., B.C., K.L., O.V.H., N.K.C.; Data Curation, K.E.P, B.C.; Writing—original draft, K.E.P. and N.K.C.; Writing—Review & Editing, K.E.P., B.C., K.L., B.P.T., N.K.C.; Visualization, K.E.P. and N.K.C.; Supervision, B.P.T., Y.X., N.K.C.; Funding Acquisition, B.P.T., Y.X., N.K.C.

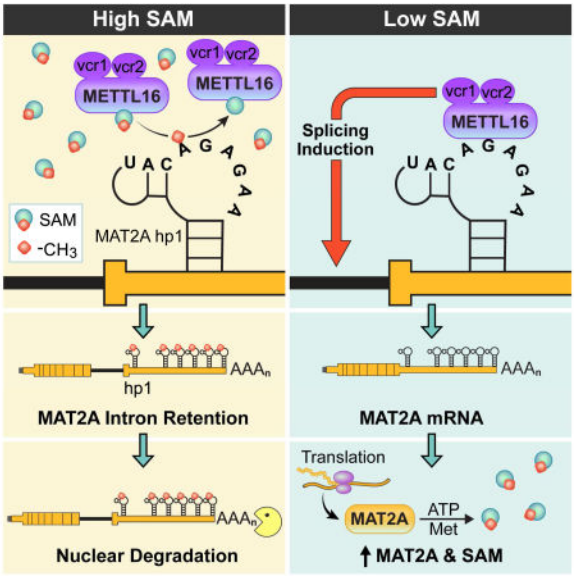

INTRODUCTION

S-adenosylmethionine (SAM) serves as methyl donor for nearly all cellular methylation reactions. The widespread use of methylation to regulate the activities of DNA, RNA, and proteins requires cells to precisely maintain SAM levels, but the mechanisms that control intracellular SAM abundance in mammalian cells are not well understood. Bacteria use riboswitches to directly link intracellular SAM levels with the production of the SAM synthetases that generate SAM from methionine (Met) and ATP (Wang and Breaker, 2008). Several observations suggest that human SAM synthetase expression is also posttranscriptionally regulated. The human MAT2A gene encodes the SAM synthetase expressed in all cells except liver cells. Upon Met depletion, the stability of the cytoplasmic MAT2A mRNA increases (Martinez-Chantar et al., 2003). Furthermore, the MAT2A 3´ UTR contains six hairpin structures that are evolutionarily conserved among vertebrates (Parker et al., 2011). While these do not bind SAM or function as a riboswitch, their conservation implies they are involved in MAT2A regulation. In addition, a significant fraction of the total MAT2A transcript accumulates in the nucleus in a retained intron isoform that is subject to nuclear degradation (Bresson et al., 2015). Intron retention in mammals is not well characterized, but recent studies suggest that it contributes to the regulation of thousands of mammalian RNAs (Boutz et al., 2015; Braunschweig et al., 2014; Yap et al., 2012). Together, these observations suggest that cells control SAM homeostasis using undefined posttranscriptional mechanisms to regulate MAT2A.

For decades, N^6-methyladenosine (m^6A) has been recognized as a common mRNA modification, but only with the introduction of transcriptomics approaches (m^6A-seq) has the full scope of m^6A targets been defined (Dominissini et al., 2012; Meyer et al., 2012; Yue et al., 2015). The catalytic METTL3 protein in complex with a catalytically inactive METTL14 and the RNA-binding protein WTAP modify most m^6A sites in mRNA (Bokar et al., 1997; Liu et al., 2014; Ping et al., 2014; Schwartz et al., 2014; Sledz and Jinek, 2016;

Wang et al., 2016a; Wang et al., 2016b). The METTL3 complex methylates mRNAs at RRACH motifs (R = A or G; H = A, C or U), often in 3′ UTRs (Dominissini et al., 2012; Ke et al., 2015; Meyer et al., 2012; Yue et al., 2015). Knockdown of the components of the METTL3 complex leads to changes in splicing patterns, alternative polyadenylation, RNA stability, transcriptional silencing, and translation (Dominissini et al., 2012; Ke et al., 2015; Lin et al., 2016; Meyer et al., 2015; Patil et al., 2016; Schwartz et al., 2014; Wang et al., 2016b; Zhou et al., 2015). Mechanistically, these changes in mRNA expression have been linked to RNA binding proteins whose affinity for a transcript is altered by m^6A modification (Alarcon et al., 2015; Dominissini et al., 2012; Du et al., 2016; Luo and Tong, 2014; Patil et al., 2016; Wang et al., 2014; Xiao et al., 2016; Zhou et al., 2015). In addition, methylation can alter protein binding by changing RNA structures (Liu et al., 2015).

Despite these advances, the understanding of m^6A pathways remains incomplete. It is unknown how, or even whether, the methylation of specific sites alters specific RNA processing events in response to intracellular or extracellular conditions. Furthermore, methyltransferases other than METTL3 contribute to the overall m^6A profile. Notably, it has been over 35 years since the discovery that the U6 snRNA is m^6A modified (Epstein et al., 1980; Harada et al., 1980). The m^6A site lies in a sequence important for splicing catalysis and it is conserved (Brow and Guthrie, 1988; Gu et al., 1996; Nguyen et al., 2016). As such, this modification may contribute to U6 snRNA function, but the identity of the methyltransferase has remained unknown.

Here, we define a posttranscriptional regulatory mechanism involving a specific m^6A methylation site and the methyltransferase METTL16 that controls MAT2A intron retention in response to intracellular SAM levels. We show that splicing of the MAT2A retained intron is rapidly induced upon Met depletion, and this effect requires a conserved hairpin (hp1), which we further show is a METTL16 m^6A substrate. Importantly, knockdown of METTL16 abrogates induction of MAT2A splicing in Met-deprived conditions, while forced binding of METTL16 to the MAT2A 3′ UTR is sufficient to promote splicing in Met-replete conditions. We propose a model in which METTL16 occupancy on MAT2A hp1 promotes splicing of the retained intron. Under high SAM levels, METTL16 binds, methylates, and disassociates rapidly to favor intron retention. In SAM-limiting conditions, METTL16 cannot methylate efficiently, which increases its dwell time on hp1 and stimulates splicing of the retained intron. Finally, we show that METTL16 is the long-unknown U6 snRNA methyltransferase, and this function is conserved in *S. pombe*. We conclude that METTL16 is the conserved U6 snRNA methyltransferase, and it has evolved an additional function in vertebrates to control SAM homeostasis by posttranscriptionally regulating SAM synthetase gene expression.

RESULTS

MAT2A Intron Retention Is Regulated

The MAT2A gene produces two RNA isoforms across multiple cell types, a cytoplasmic mRNA and a nuclear retained-intron isoform (MAT2A–RI)(Figure 1A and S1A)(Bresson et al., 2015). Because MAT2A mRNA levels increase in Met-free media (Martinez-Chantar et al., 2003), we tested whether Met depletion regulates MAT2A intron retention. We observed

a rapid decrease in MAT2A–RI and an increase in MAT2A mRNA upon Met withdrawal (Figure 1B). Nuclear run-on analysis confirmed that transcription rates of MAT2A are not enhanced upon Met depletion (Figure S1B). The MAT2A protein uses Met as a substrate to produce SAM, so the increase of MAT2A mRNA is unlikely to result directly from Met depletion. Instead, several observations suggest the response is due to loss of SAM. First, heterologous overexpression of MAT2A increased SAM levels (Figure S1C), which correlated with increases in intron retention (Figure 1C). Furthermore, this effect was reversed by Met depletion, except at the highest levels of MAT2A expression. In this case, excessive SAM buildup in these cells precluded SAM depletion during the 6-hr Met deprivation (Figure S1C). Second, the MAT2A inhibitor cycloleucine decreased intron retention in Met-replete media (Figure S1D)(Coulter et al., 1974). Third, transient permeabilization to allow entry of the otherwise cell-impermeable SAM restored basal levels of intron retention in Met-depleted cells (Figure S1E). Together, these data suggest that intracellular SAM levels regulate MAT2A intron retention. Finally, we confirmed that induction of MAT2A splicing results in changes in protein levels. Because depletion of Met removes an essential amino acid, we examined MAT2A RNA and protein over a series of Met concentrations. We observed a sharp shift to the spliced mRNA isoform between 11–33 μM extracellular Met and concomitant increases in protein levels of MAT2A (Figure 1D). We conclude that MAT2A intron retention is regulated in response to SAM availability to control MAT2A protein production.

MAT2A Hairpin 1 Is Necessary for the Regulation of Intron Retention

The MAT2A 3′ UTR contains six hairpins with vertebrate-conserved sequence, structure, and placement (Parker et al., 2011). The hairpins are predicted form a “duckbill”-like stem-loop with the nearly invariant sequence “UACAGAGAA” in the loop (Figure 2A). The first hairpin lies close to the stop codon and a cluster of three to five hairpins is located further downstream (Figure 1A and Figure S2A). Given its conservation and proximity to the retained intron, we hypothesized that MAT2A hp1 regulates intron retention.

We made a series of reporter constructs with the MAT2A exon 8, intron 8, exon 9, and 3′ UTR fused to β-globin with alterations the in hp1 or the hp2–6 cluster sequences (Figure 2B). Like the endogenous RNA, the wild-type (WT) reporter responded to Met depletion by reducing intron retention and increasing mRNA (Figure 2C). Alterations in hp1 impaired splicing induction as assessed by the percent intron retention (Figure 2C) and by the steady-state levels of the intron-retained reporter RNA (Figure S2B). Mutations in the hp2–6 cluster increased the mRNA isoform under Met-replete conditions without affecting intron retention (Figure S2C), potentially due to an increase in the stability of the otherwise unstable MAT2A mRNA. More importantly, a wild-type hp1 conferred regulated intron retention in the hp2–6 mutants (Figure S2C). These observations suggest that hp1 and the conserved UACAGAGAA play critical roles in the induction of splicing of the MAT2A retained intron.

MAT2A Hairpin 1 Is M^6A Modified at a Site Identical to the U6 snRNA Methylation Site

The UACAGAGAA nonamer is identical to a sequence in U6 snRNA that is m^6A methylated by an unknown methyltransferase at position A4 (Figure 2A)(Epstein et al., 1980; Harada et al., 1980). Publically available m^6A-seq data suggest at least one METTL3-

independent m^{6}A modification near MAT2A hairpins (Dominissini et al., 2012; Linder et al., 2015; Schwartz et al., 2014). To test hairpin methylation, we performed an m^{6}A-immunoprecipitation (m^{6}A-IP) using β-globin reporter RNAs (Figure 2D). We cleaved the 5´ end of β-globin using oligonucleotide-directed RNase H to eliminate a known β-globin m^{6}A site, and this fragment served as an m^{6}A-IP positive control (Figure 2D, bottom panel). We observed efficient m^{6}A-IP of the WT and hp1 mutant RNAs and reduced efficiency for the hp2–6 cluster mutant. Importantly, mutating all six hairpins resulted in the complete loss of m^{6}A-IP of the 3´ UTR without affecting the β-globin control (Figure 2D). Thus, the UACAGAGAA sequences in the MAT2A hairpins are important for the methylation of the MAT2A 3´ UTR.

Sequence identity suggests that MAT2A hp1 is methylated at position A4 by the same machinery that methylates U6 snRNA (Figure 2A). We examined hp1 methylation in an *in vitro* assay that supports U6 snRNA methylation but not methylation of METTL3 substrates (Shimba et al., 1995). We incubated uniformly adenosine-labeled substrates in nuclear extract and monitored m^{6}A modification by P1 nuclease treatment and thin layer chromatography (TLC)(Figure 2E). Both U6 snRNA and the hp1 wild-type substrates were methylated in a SAM-dependent fashion. However, a substrate that mutates the predicted methylation site (hp1-A4G) was not methylated, nor was a METTL3 substrate (Figure 2E) (Liu et al., 2014). In addition, we site-specifically radiolabeled hp1 A2, A4, A6, A8, or A9, by splint ligation and only hp1-A4 was methylated (Figure 2F). Moreover, point mutants that interfere with splicing (Figure 2C) disrupted methylation *in vitro* (Figure 2G). We conclude that MAT2A hp1 is a substrate for m^{6}A modification at position A4 and that the U6 snRNA methyltransferase is likely responsible for the modification.

METTL16 Methylates MAT2A Hairpins and Contributes to Splicing Induction

The conserved METTL16 protein contains a methyltransferase domain and two vertebrate-conserved regions (Figure S3A). The *E. coli* homolog of METTL16 m^{6}A methylates rRNA within a CAG motif, consistent with the site in U6 snRNA and MAT2A (Sergiev et al., 2008). Interestingly, *S. pombe* encodes a METTL16 homolog, and its U6 snRNA is m^{6}A methylated (Gu et al., 1996). However, *S. cerevisiae* does not encode a METTL16 homolog and, to our knowledge, budding yeast U6 snRNA is not methylated. Moreover, METTL16 is nuclear, consistent with a role in regulation of MAT2A splicing and U6 methylation (Brown et al., 2016). For these reasons, we explored the possibility that METTL16 methylates MAT2A and U6 snRNA.

Several observations demonstrate that METTL16 is necessary for efficient MAT2A splicing and that this contributes to MAT2A activity. First, knockdown of METTL16 with siRNA (siM16) increases intron retention in the presence of Met (Figure 3A, S3B and S3C). Second, MAT2A–RI levels did not decrease significantly upon Met depletion and a highly attenuated increase in spliced mRNA was observed in the siM16-treated cells (Figure 3A and S3D). Third, MAT2A protein levels decreased ~26% upon METTL16 knockdown (Figure S3C). Fourth, as described in more detail below, SAM levels and m^{6}A/A ratios decreased upon METTL16 knockdown (Figure 6A and 6B). Thus, METTL16 is necessary for the regulation of MAT2A by intron retention.

We next tested whether METTL16 methylates MAT2A hp1. MAT2A contains a METTL3-dependent m^6A site upstream of the 3′ UTR (Linder et al., 2015). We liberated hp1 from this site by RNase H treatment of RNA from siCtrl or siM16-treated cells (Figure 3B, top). We performed m^6A-IP and found that MAT2A hp1 and coding sequence (CDS) efficiently immunoprecipitated from the siCtrl cells, but only the CDS immunoprecipitated in the siM16-treated cells (Figure 3B). We next confirmed a physical interaction between METTL16 and the MAT2A hairpins using formaldehyde-crosslinked RNA-immunoprecipitation (RIP)(Conrad, 2008). Cell lysates from crosslinked or non-crosslinked controls were briefly treated with nuclease and immunoprecipitated with anti-METTL16 antibody. Only hp1 and the hairpin cluster region of MAT2A were enriched in the crosslinked METTL16 IP (Figure 3C, Figure S3E). Thus, METTL16 interacts with the MAT2A hairpin regions and is required for their methylation in cells.

To examine the biochemical activity of METTL16, we immunodepleted METTL16 from nuclear extract and tested methylation of hp1 (Figure 3D and S3F). We observed a nearly 6-fold decrease in methylation of hp1 in METTL16-immunodepleted extracts. Purified recombinant METTL16 methyltransferase domain (rM16-MTD; Figure S3G) increased activity in immunodepleted and control extracts. Furthermore, hp1 methylation activity was robust on the anti-METTL16 beads and virtually undetectable in the control beads. In addition, rM16-MTD was sufficient to specifically methylate hp1-A4, but none of the other hp1 adenosines (Figure 3E). Moreover, two recombinant proteins with mutations of highly conserved residues in the substrate-binding domain abrogated the activity (PP185/186AA and F187G)(Malone et al., 1995). Finally, rM16-MTD was unable to methylate two mutants that reduced splicing in reporter assays (Figure 3F). We conclude that METTL16 is required for induction of MAT2A splicing and it methylates the UACAGAGAA sequence in MAT2A 3′ UTR hairpins.

METTL16 Occupancy of Hairpin 1 Promotes MAT2A Splicing

Met depletion, hp1 mutation, or METTL16 knockdown reduce MAT2A hairpin modification (Figure S4A, 2D, and 3B), but the consequences of these treatments differ. Met depletion increases MAT2A mRNA (Figure 1B), while hp1 mutation or METTL16 knockdown results in loss of induction of splicing and mRNA production (Figure 2C and 3A). To rationalize this apparent contradiction, we hypothesized that the dwell time of METTL16 on hp1 dictates MAT2A splicing efficiency. In Met-rich conditions, SAM is plentiful, and METTL16 briefly occupies hp1 due to enzyme turnover. In Met-deprived conditions, the lack of SAM slows methylation and prolongs METTL16 occupation of hp1, which then drives splicing of MAT2A intron eight (Figure 7).

In this model, the methyltransferase activity regulates the dwell-time of METTL16 on MAT2A 3′ UTR, but methylation is not directly required for splicing. The model predicts that overexpressing wild-type or catalytically inactive METTL16 should drive hp1 binding and promote splicing even in Met-replete conditions, but an RNA-binding mutant should not induce splicing. Both the METTL16 PP185/186AA and F187G mutants are catalytically inactive (Figure 3E). In native RIP experiments, F187G does not bind MAT2A while the PP185/186AA mutant binds MAT2A, albeit less efficiently than wild-type METTL16

(Figure S4B, S4C). We knocked down endogenous METTL16 and overexpressed siRNA-resistant METTL16 wild-type, PP185/186AA, or F187G. As predicted, overexpression of wild-type METTL16 or PP185/186AA decreased intron retention in both Met-depleted and Met-rich media, whereas the RNA-binding mutant F187G did not affect intron retention (Figure 4A). Importantly, all three proteins were overexpressed to similar levels (Figure S4D). To verify the role of hp1, we performed a similar experiment with the β-MAT-WT or β-MAT-hp1-C3G reporters (Figure 4B). Once again, we observed decreased intron retention in the β-MAT-WT reporter upon METTL16 and PP185/186AA overexpression, but no change upon F187G overexpression. Overexpression of these proteins had little effect on intron retention in the β-MAT-hp1-C3G, demonstrating that hp1 is essential for splicing induction. These results suggest that METTL16 binding, but not methylation activity, is required for the induction of MAT2A splicing.

To further test the role of METTL16 occupancy on MAT2A splicing, we employed an MS2-tethering assay. We placed a binding site for the bacteriophage MS2 coat protein downstream of a mutant hp1 and co-expressed MS2 fusions to wild-type or F187G METTL16 (Figure 4C). Importantly, the point mutation, hp1-A4G, abrogates binding of METTL16 (Figure S4E). If METTL16 occupancy is the key to MAT2A splicing, tethering should be sufficient to induce splicing in the presence of Met and complement the lack of activity of the F187G and hp1 mutants (Figure 4A and 4B). Indeed, tethering of wild-type or F187G METTL16 was sufficient to drive splicing in a hp1 mutant reporter, but MS2-alone, MS2-hnRNP A1 and MS2-hnRNP C1 negative controls were not (Figure 4C). METTL16 homologs are found from *E. coli* to humans, but the MAT2A hairpins and two carboxyl-terminal METTL16 vertebrate conserved regions (VCRs) are restricted to vertebrates (Figures S3A). We reasoned that the METTL16-VCRs may promote splicing, while the methyltransferase domain regulates association with the transcript. Consistent with this hypothesis, tethering the METTL16-VCRs was sufficient to drive splicing, but the methyltransferase domain was not (Figure 4C). We conclude that METTL16 binding is sufficient to promote MAT2A splicing through the METTL16-VCR domains.

Finally, we performed a native RIP to monitor METTL16-MAT2A RNA association. As expected, METTL16 immunoprecipitated with MAT2A more efficiently after Met depletion (Figure 4D and S4F), further supporting the idea that METTL16 occupancy increases upon Met depletion to enhance MAT2A splicing. Taken together, these data strongly support the conclusion that METTL16 binding to hp1 drives splicing of the MAT2A retained intron. Moreover, they suggest that the METTL16 methyltransferase domain controls binding to hp1, but the METTL16-VCRs promote splicing.

METTL16 Is the U6 m^{6}A-Methyltranfserase

The similarity between the MAT2A hairpin and U6 snRNA methylation sites suggest that METTL16 is the U6 snRNA methyltransferase. However, U6 snRNA adopts a variety of intermolecular and intramolecular structures, but none obviously resemble the MAT2A hairpin “duckbill” (e.g. Figure S5A). In principle, the duckbill may not be required for hp1 methylation, but individual mutation of each of the four bases that comprise the duckbill reduced methylation (Figure 5B compare lane 1 with lanes 2, 3, 5, and 6). However,

compensatory mutations that restore base pairing did not restore activity (Figure 5B, lanes 4 and 7; Figure S5B), demonstrating that a two-nucleotide base pair at this position is not sufficient for activity. Instead, METTL16 may require a sequence-specific 2-nt base pair or the upstream GU may contribute to methylation as a sequence-specific single-stranded dinucleotide. If U6 snRNA is a METTL16 substrate, these findings suggest that it will have a similar upstream GU sequence or a two-nucleotide base paired structure adjacent to the methylated adenosine.

We first used biochemical assays to confirm that METTL16 is the U6 snRNA methyltransferase. We incubated rM16-MTD with U6 snRNA radiolabeled at position A43, which corresponds to A4 in the UACAGAGAA sequence (Figure 5A, S5A). As predicted, rM16-MTD methylates U6 snRNA A43, while PP185/186AA and F187G do not (Figure 5C). In METTL16 immunodepletion experiments, we observed reduced methylation, complementation by rM16-MTD, and robust activity on the anti-METTL16 beads (Figure 5D) further confirming that METTL16 methylates U6 snRNA at A43. Unlike hp1, there is no GU dinucleotide upstream of the methylation site. However, the AC preceding the m^6A site is base paired with G88 and U89 similar to G(−6) and U(−5) in hp1 (Figure 5A and S5A)(Mougin et al., 2002). We observed no methylation of G88C substrates with rM16-MTD or nuclear extract (Figure 5C and Figure S5C). In addition, mutation of the bases immediately preceding G88 did not affect methylation, demonstrating the specificity of the G88C mutation (Figure S5C). Thus, both G88 in U6 snRNA and G(−6) in hp1 are essential for methylation by METTL16. Their primary sequence positions relative to the site of methylation are quite different, but the secondary sequences are similar (Figure 5A). Taken together, these data suggest that METTL16 prefers a substrate in which the AC flanking of the methylated adenosine is base-paired with GU.

In addition to these biochemical data, we observed an interaction between METTL16 and U6 snRNA in cells, but not U1 snRNA or 7SK RNA controls (Figure 5E, Figure S5D). Surprisingly, we observed no change in U6 snRNA m^6A-IP efficiency upon METTL16 knockdown (data not shown). We reasoned that the long half-life of U6 snRNA and residual METTL16 activity after knockdown masked differences in steady-state U6 snRNA methylation. A published CRISPR screen and our failed attempts to knockout METTL16 suggest that METTL16 is essential in mammalian cells (Wang et al., 2015). However, deletion of the *S. pombe* METTL16 homolog, Duf890, produces viable, albeit slow-growing, yeast. M^6A-IP of U6 snRNA was lost on RNA from two independent ΔDuf890 colonies, but m^6A-IP of the U2 snRNA control was unaltered (Figure 5F). We conclude that METTL16 and its eukaryotic homologs are U6 snRNA m^6A methyltransferases.

Identification of METTL16-dependent m^6A sites

The METTL3 complex is responsible for the majority of mRNA methylation on the degenerate consensus RRACH. In contrast, methylation of U6 snRNA and MAT2A apparently requires both the UACAGAGAA nonamer and a specific RNA structure. These observations suggest that METTL16 is not a widely used mRNA m^6A methyltransferase. However, we observed an ~20% drop in m^6A to A ratios upon METTL16 knockdown (Figure 6A). In principle, METTL16 could frequently target UACAGAGAA sequences, or

its activity could be expanded to non-UACAGAGAA targets by unknown cellular co-factors. Alternatively, METTL16 knockdown may lower m^{6}A by decreasing MAT2A activity. In fact, SAM levels were reduced in siM16-treated cells (Figure 6B). In the latter case, METTL16 contributes globally to m^{6}A methylation through its role in SAM biosynthesis.

To explore these potential broader roles for METTL16, we performed m^{6}A-seq and identified 2,715 peaks in 1533 genes that decrease upon METTL16 knockdown (Table S1). In contrast to typical m^{6}A sites commonly found in 3′ UTRs, 82% of the METTL16-dependent peaks were in introns or spanned intron-exon boundaries (Figure 6C). Compared to introns as a whole, this subset had a higher GC content, were shorter, and they skewed slightly to the 3′ ends of the RNAs (Figure S6A). Thus, the METTL16-sensitive peaks represent a distinct subset of m^{6}A modifications.

Only MAT2A and two additional peaks overlapped an UACAGAGAA site (GNPTG and GMIP; Figure 6D). Unlike MAT2A, we observed no METTL16 binding in cells and no methylation of these additional sites in nuclear extract (Figure 6E and 6F, lanes 1–3). Furthermore, the UACAGAGAA sequences are not conserved (Figure S6B), and there is a verified RRACH methylation site within the GNPTG peak (Linder et al., 2015). In addition, we examined the m^{6}A IP efficiency of all windows that contain UACAGAGAA sites and have reads in the siCtrl m^{6}A-IP sample (Table S2). We observed no differences upon METTL16 knockdown between this dataset and two randomized control groups (Figure S6C). We conclude that UACAGAGAA element is not widely methylated by METTL16.

To test whether METTL16-dependent peaks respond to SAM levels, we knocked down or overexpressed MAT2A and performed m^{6}A-IP on several METTL16-dependent and METTL16-independent m^{6}A sites (Figure 6G, 6H, S6D, S6E). Upon MAT2A knockdown, the m^{6}A-IP efficiency of the METTL16-dependent sites decreased compared to the METTL16-independent sites (Figure 6G), while MAT2A overexpression increased METTL16-dependent m^{6}A-IP efficiency (Figure 6H). These data support the conclusion that METTL16-dependent m^{6}A sites are sensitive to SAM levels. Surprisingly, MAT2A overexpression was not able to complement METTL16 depletion (Figure 6I), suggesting that their METTL16-dependence is not exclusively the result of depressed SAM levels. However, we observed no binding to METTL16 (Figure 6J) and no methylation of three strong candidates in vitro (Figure S6F and 6F, lanes 4–7), suggesting they are not direct targets (see Discussion). Regardless of whether these are direct or indirect targets of METTL16, these data show that METTL16 is required for normal m^{6}A methylation profiles beyond its direct effects on the methylation of U6 snRNA and MAT2A.

DISCUSSION

Precise control of SAM levels is important for a variety of cell functions, but SAM regulation is not well understood. Our data suggest a model in which METTL16 occupancy of hp1 controls production of SAM by inducing splicing of the MAT2A retained intron in SAM-limiting conditions (Figure 7). When SAM is available (top), METTL16 binds hp1, methylates it, and then disassociates. Although limited basal splicing likely occurs, the short dwell time of METTL16 is insufficient for robust splicing induction. The nuclear MAT2A–

RI is then degraded by PABPN1-PAPα/γ mediated RNA decay (Bresson et al., 2015). In SAM- limiting conditions (bottom), METTL16 binds to hp1, but stalls due to the lack of a methyl donor. The resulting increased occupancy on hp1 stimulates splicing of the MAT2A retained intron through the METTL16-VCRs. For simplicity, the diagram depicts posttranscriptional splicing induction, but we favor a model in which METTL16 promotes co-transcriptional splicing induction. We propose that METTL16 is a central factor in a feedback loop that links SAM levels to expression of the SAM synthetase.

Methylation of mRNA affects RNA processing at multiple stages of gene expression. Generally, m^6A mechanisms involve methylation "writers" (e.g. METTL3) that add the modification and "readers" (e.g. YTH family proteins) that differentially bind methylated RNA to induce changes in RNA metabolism (Yue et al., 2015). This work expands the mechanistic understanding of m^6A modification in two important ways. First, it has been difficult to directly link an intracellular or extracellular signal to a change at a specific m^6A site that in turn alters expression the modified mRNA. Here we link intracellular SAM levels with methylation of a specific adenosine in MAT2A that subsequently regulates intron retention. Second, in contrast to the two-component writer-reader paradigm, METTL16 serves as both m^6A writer and reader. Interestingly, METTL3 binding to 3′ UTRs can promote translation independent of m^6A methylation (Lin et al., 2016). Thus, while m^6A generally affects RNA metabolism through methylation readers, direct contributions of methyltransferases on RNA processing should not be overlooked.

Precisely how METTL16 promotes splicing remains unknown and unidentified co-factors certainly contribute to splicing induction. The UACAGAGAA element in U6 snRNA is critical for pre-mRNA splicing (Brow and Guthrie, 1988; Gu et al., 1996; Nguyen et al., 2016), so it is tempting to speculate that this sequence is used as a U6 mimic to regulate splicing of the retained intron. In principle, the methylation of U6 snRNA could be linked to splicing induction, but this seems unlikely, as the steady-state U6 snRNA methylation state does not change rapidly enough to account for the quick changes in splicing of MAT2A. Regardless of the potential roles for U6 snRNA, our data show that stable association of METTL16 is a key point of regulation of MAT2A splicing. The tethering assays further show that the METTL16-VCRs are sufficient to promote splicing, consistent the vertebrate co-evolution of the hairpins and these domains. Future studies will seek to define the mechanisms of METTL16-induced MAT2A splicing.

METTL16 homologs are found in organisms ranging from *E. coli* to humans, but little is known about their functions. With the exception of rRNA targeting by *E. coli* ybiN/rlmF, no substrates for METTL16 family members have previously been identified (Sergiev et al., 2008). The *C. elegans* METT-10 restricts germ cell proliferation and is important for development of several organs (Dorsett et al., 2009), and *A. thaliana* FIONA1 is essential for maintaining plant circadian rhythms (Kim et al., 2008). The *C. elegans* and *A. thaliana* SAM synthetase genes have no UACAGAGAA elements, so these phenotypes are likely attributable to loss of U6 snRNA methylation, methylation of an unidentified target(s), or even other unknown functions of METTL16. In fact, while this work was under review, METTL16 was reported to bind a structured 3′-end triple helix structure of the nuclear noncoding MALAT1 RNA, apparently independent of its methyltransferase activity (Brown

et al., 2016). The substrate specificities of METTL16 family members suggest that they evolved initially to be rRNA methyltransferases and subsequently were co-opted by eukaryotes to target U6 snRNA. Later, vertebrate METTL16 gained a second function in the regulation of SAM using the METTL16-VCRs and the hairpin loops in MAT2A.

Our m^{6}A-seq identified a large number of METTL16-dependent m^{6}A sites. We cannot determine conclusively from our data whether METTL16 directly targets these sites or they are strictly regulated by the loss of intracellular SAM (Figure 6B). Consistent with the sites being indirect, the UACAGAGAA consensus was not enriched, METTL16-dependent m^{6}A sites are sensitive to SAM levels (Figure 6G, 6H, S6E), no interaction was observed by RIP (Figure 6J), and putative targets were not methylated *in vitro* (Figure 6F). However, METTL16 knockdown was not complemented by increasing SAM levels by overexpression of MAT2A, supporting a more direct role for METTL16 in these m^{6}A peaks (Figure 6I, S6E). Therefore, our data do not rule out the model that METTL16 methylates these sites, perhaps using different cellular co-factors that direct its activity to sites lacking the UACAGAGAA sequence. Importantly, even if the sites identified here are indirect, other direct targets of METTL16 may exist. For example, our poly(A)-selection step excludes detection of non-polyadenylated RNAs, and our bioinformatic pipeline filters any peaks lost in the METTL16 knockdown samples that are also down-regulated in the input samples.

Regardless of whether the METTL16-dependent peaks are indirect or direct METTL16 targets, our analysis revealed a distinct subset of m^{6}A sites. Unlike the m^{6}A sites commonly found in UTRs, the METTL16-dependent sites were primarily localized to introns or intron-exon boundaries. Because we selected for poly(A), these are likely intron-retained RNAs. Moreover, the introns themselves were on average shorter and more GC-rich. Interestingly, short, GC-rich introns have been reported to be more subject to intron retention and may be spliced by intron definition (Amit et al., 2012). Whether METTL16-dependent m^{6}A methylation is mechanistically linked to these splicing characteristics remains unknown. We also cannot rule out confounding effects that loss of U6 snRNA methylation may have on splicing or biogenesis of methylated pre-mRNAs. In any case, further definition of the mechanisms METTL16 will lead to insights into SAM homeostasis and RNA biogenesis.

STAR Methods

Contact for Reagent and Resources Sharing

Nicholas K. Conrad

Department of Microbiology, UT Southwestern

Nicholas.Conrad@utsouthwestern.edu

Experimental Model and Subject Details

Cell culture procedure—HEK293 and HEK293T cells were grown at 37°C in DMEM (Sigma) supplemented with 10% FBS (Sigma), penicillin-streptomycin, and 2mM L-glutamate. 293A–TOA cells were cultured in the same conditions, but Tet-Free FBS (Atlanta Biologicals) was used instead. Methionine-free DMEM (Thermo Fisher 21013024) was

additionally supplemented with 1mM sodium pyruvate and 0.4mM L-cysteine (Sigma). Due to SAM sensitivity of MAT2A splicing, care was taken to use fresh media so Met levels would not be depleted. When necessary, we supplemented Met and/or changed media, as specified for each assay.

Yeast strains—Haploid yeast strain agar stabs (ΔDuf890/SPAC27D7.08c and wild-type/ED666) were purchased from Bioneer. The ΔDuf890 strain was grown in YES media supplemented with 100μg/mL G418 at 30°C. Wild-type was grown in YES media without G418 at 30°C.

Methods Details

Transfection—Cells were transfected using TransIT-293 (Mirus) according to the manufacturer's protocol. For a typical 12-well transfection, 2μL of TransIT-293 was mixed with 40μL Opti-MEM (Thermo Fisher) and incubated for 5 minutes at room temperature. This mixture was then added to 800ng of DNA and incubated for 15 minutes before adding to cells. For the reporter assays, we generally used 30ng of β-globin reporter plasmid balanced with 770ng pcDNA3. METTL16 expression plasmids were added as indicated. In the MS2 reporter assays, 15ng of the β-globin reporter was used with 200ng of the MS2-METTL16 plasmid and 585ng of pcDNA3.

siRNA knockdown experiments—293A–TOA cells were transfected with 30nM siRNA for METTL16 knockdowns (15nM of siMETTL16-1 and 15nM of siMETTL16-2) and 20nM siRNA for MAT2A knockdowns (Thermo Fisher) using RNAiMax transfection reagent (Thermo Fisher) according to the manufacturer's instructions. Twenty-four hours following transfection, ~100% confluent cells were diluted to new plates to allow the cells to divide for an additional 72 hours (total 96 hour knockdown).

For puromycin-resistant rescue, we transfected HEK293T cells with siMETTL16-2 at 20nM. After 24 hours of knockdown, ~100% confluent cells were diluted to new 6-well plates to allow the cells to divide for an additional 72 hours. The next day, we transfected 1μg of siRNA Resistant FLAG-METTL16 plasmid (or pcDNA3-Flag control) with 1μg of pX459 of puromycin-resistance plasmid into the cells. 12 hours later, 3μg/mL of puromycin was added to the media. At 48 hours after plasmid transfection (96 hours of knockdown), we changed to +/− L-methionine media for 4 hours.

Cycloleucine—Cycloleucine (Sigma) was resuspended in H_2O at 300 mM and added to cell media at a final concentration of 30 mM.

Methionine depletion—For methionine depletion, cells were washed two times with Dulbecco's Phosphate Buffer Saline (PBS) with calcium chloride and magnesium chloride (Sigma). Media was then replaced with supplemented Met-free media. 100μM of L-methionine (Sigma) was supplemented as appropriate. Depletion typically occurred from 4–6 hours (specified in experiments).

SAM replacement by Digitonin Permeabilization—293A–TOA cells were grown to ~95% confluency in a 12-well plate. Cells were washed twice with PBS with calcium

chloride and magnesium chloride. Media was then replaced with Met-free media supplemented with Met as indicated. After 4 hrs, cells were washed once with PBS with calcium chloride and magnesium chloride and 800μL of digitonin permeabilization solution (50mM HEPES pH7.0, 100mM KCl, 85mM sucrose, 3mM $MgCl_2$, 0.2% BSA, 1mM ATP, 0.1mM DTT, 10μg/mL digitonin)(Orzalli et al., 2015) was added to cells and supplemented with 100μM L-methionine or S-adenosylmethionine as appropriate. After 10 minutes, permeabilization solution was aspirated from cells, and Met-free media was reapplied to cells, supplemented to 100μM L-methionine or S-adenosylmethionine as appropriate. Cells were kept in this media for another 2 hours then harvested with Trizol.

Northern blotting—Northern blots were performed using standard techniques with RNA probes. The RNA probes were generated from PCR products with a T7 RNA polymerase promoter; primers are listed in Table S3. Alternatively, probes were made from a digested plasmid. For some northern blots, 35–100 μg of total RNA were selected on Sera-Mag Oligo (dT)-Coated Magnetic particles (GE Healthcare Lifesciences) to enrich for polyadenylated RNAs prior to gel electrophoresis.

Cell fractionation—For a 6-well plate, cells were trypsinized, pelleted for 3 min at 700 × g at 4°C, washed with cold PBS , and pelleted again. PBS was removed, and then pellets were resuspended in 100μL ice cold Buffer I (10mM Tris-HCl pH 8.0, 0.32M Sucrose, 3mM $CaCl_2$, 2mM magnesium acetate, 0.1mM EDTA, 0.5% Triton X-100, 4U RNasIn Plus (Promega), 1mM DTT) and incubated on ice for 5 min Cells were then pelleted by centrifugation at 500xg at 4°C for 5 min The supern atant was added to 1mL TriReagent (Molecular Research Center) for cytoplasmic fraction. The pellet was resuspended in Buffer I-150 (150mM NaCl, 10mM Tris-HCl pH 8.0, 0.32M Sucrose, 3mM $CaCl_2$, 2mM magnesium acetate, 0.1mM EDTA, 0.5% Triton X-100, 4U RNasIn Plus, 1mM DTT) and pelleted by centrifugation at 500xg at 4°C for 5 min The supernatant was discarded. The pellet was resuspended in Buffer I and 1mL of TriReagent for the nuclear fraction.

Quantitative RT-PCR—RNA was harvested using TriReagent according to the manufacturer's protocol. Following extraction, RNA was treated with RQ1 DNase (Promega). Random hexamers were used to prime cDNA synthesis with MuLV reverse transcriptase (New England Biolabs). Real-time reactions used iTaq Universal SYBR Green Supermix (Biorad). Primers are listed in Table S3; if primer efficiencies are not listed they were assumed to be 100%.

Nuclear run-on assay—Nuclear run-ons were performed essentially as previously described (Stubbs and Conrad, 2015). Two 15cm plates of HEK293 cells at ~90% confluency were used per sample. Cells were incubated in media +/− L-methionine for 2 or 6 hours. Cells were trypsinized, quenched with ice-cold media, and pelleted at 700xg for 3min at 4°C. Pellets were then rinsed wit h ice-cold PBS and collected by centrifugation. Cells were resuspended in 1mL HLB buffer (10mM Tris-HCl pH 7.5, 10mM NaCl, 2.5mM $MgCl_2$, 0.5% Igepal CA-630, 1mM DTT) and incubated on ice for 5min The solution was underlaid with 1mL HLB-Sucrose (10mM Tris-HCl pH 7.5, 10mM NaCl, 2.5mM $MgCl_2$, 0.5% Igepal CA-630, 1mM DTT, 10% Sucrose). The sample was centrifuged at 600xg for

5min at 4°C. Th e supernatant was discarded. Nuclei were isolated and resuspended in an equal volume of transcription reaction buffer (10mM Tris pH 8.0, 90mM KCl, 5mM $MgCl_2$, 25% glycerol, 2.5mM DTT), and an NTP mix containing 4-thio-UTP or rUTP (10mM rATP, rGTP, rCTP, 40μM 4-thio-UTP/rUTP) was added. Transcription proceeded at 30°C for 5 min and the reaction was quenched with 1mL TriReagent. RNA was extracted, biotinylated, then streptavidin selected. Quantitative RT-PCR was used to evaluate the results.

RNase H Procedure—For 10μg of RNA, RNA pellet suspended in 10μL of water and 1μM of DNA oligonucleotide was added. The mixture was heated to 65°C for 5 min, then the heat block was allowed to slow cool to 37°C. 1x RNaseH Buffer (20mM Tris-HCl pH 7.5, 100mM KCl, 10mM $MgCl_2$), 10mM DTT, 8U RNaseIn Plus, 0.5U RNaseH (Promega) was added to the RNA mixture. This solution was incubated at 37°C for 1 hour. The reaction was quenched with 180μL of G-50 Buffer (20mM Tris-HCl pH 6.8, 300mM sodium acetate, 2mM EDTA, and 0.25% SDS), phenol:chloroform:iso-amyl alcohol (25:24:1) (PCA) extracted, and ethanol precipitated. Oligonucleotides used are listed in Table S3.

Formaldehyde RIP—Formaldehyde RIP was performed as described in (Conrad, 2008) with a few changes. One 15-cm plate of ~95% confluent HEK293T cells was used for each sample. For crosslinked samples, PBS was supplemented with 0.1% methanol-free formaldehyde (Electron Microscopy Sciences), and 15mL of this solution was applied to the plates with gentle rocking for 10 min Non-crosslinked samples underwent the same treatment with PBS lacking formaldehyde. The reaction was quenched with 1.875mL of 2M Glycine (pH 7.0) per plate. Cells were scraped, then centrifuged at 700×g for 3 min at 4°C. Cells were resuspended in 10mL of ice-cold PBS and centrifuged again. Pellets were resuspended in 1mL of ice-cold PBS, transferred to a microcentrifuge tube, centrifuged at 2400×g for 1min, and the PBS was aspirated. Pellets were resuspended in 400μL of RIPA-Plus Buffer (1% Igepal CA-630, 0.5% sodium deoxycholate, 0.1% SDS, 150mM NaCl, 50mM Tris-HCl pH 8.0, 2mM EDTA, 1x PMSF (Sigma), 1x protease inhibitor cocktail V (Fisher Scientific), 0.1μg/mL competitor RNA, 10U RNasIn Plus). DNA was sheared using a QIAShredder (Qiagen). Next, $CaCl_2$ was added to 5mM with 30U of RQ1 DNase and incubated for 15 min at 25°C. For RNA digestion, Mi crococcal Nuclease (New England Biolabs) was diluted to 10 gel units/μL in RIPA buffer and 5μL of this freshly diluted 1:200 stock was added to the extract. RNA digestion proceeded at 25°C for precis ely 10 min, after which 50μL of 300mM EGTA was added to stop the reaction. After clarification of the lysate by two successive centrifugation steps at 16000 × g for 10 min, the METTL16-RNA complexes were immunoprecipitated overnight with anti-METTL16 or mouse IgG1 antibody. Twenty-five μL of washed Protein A Dynabeads (Invitrogen) were added to each sample for one hour the following day. Beads were washed once with ice-cold RIPA, then twice by adding RIPA-U (1% Igepal CA-630, 0.5% sodium deoxycholate, 0.1% SDS, 150mM NaCl, 50mM Tris-HCl pH 8.0, 2mM EDTA, 1M Urea) to the beads and nutating them for 10min at room temperature, and once more with ice-cold RIPA. The beads were resuspended in 130μL of reverse buffer (10mM Tris-HCl pH 6.8, 5mM EDTA, 10mM DTT, 1% SDS) and heated for 45min at 70°C. Proteins were digested by adding 150μL of a 2x proteinase K solution (0.2mg/mL Proteinase K, 40mM Tris-HCl pH 7.5, 5mM EDTA, 0.2mg/mL competitor RNA) followed by 30min incubation at 37°C. Following digestion,

the samples underwent PCA extraction and ethanol precipitation. The resulting RNA was used for quantitative RT-PCR.

Native RIP—Native RIP was performed based on the cell mixing experiments in (Conrad, 2008). One 15-cm plate of ~95% confluent HEK293T cells was used for each sample. Media was changed on the cells to +/−methionine for 6 hours prior to harvest. Cells were harvested by trypsin, quenched with media, and washed with PBS. Pellets were then resuspended in 400μL RSB100-T (10mM Tris-HCl pH 7.5, 100mM NaCl, 2.5mM $MgCl_2$, 0.5% Triton X-100) supplemented with protease inhibitors and RNasIn Plus. Next, $CaCl_2$ was added to 5mM with 45U of RQ1 DNase and incubated for 15 min at 25°C. For RNA digestion, Micrococcal Nuclease was diluted to 10 gel units/μL in RIPA buffer and 10μL of this freshly diluted 1:200 stock was added to the extract. RNA digestion proceeded at 25°C for precisely 10 min, after which 50 μL of 300mM EGTA was added to stop the reaction. After clarification of the lysate by centrifugation at 10000 × g for 10 min, the METTL16-RNA complexes were immunoprecipitated for 1 hour with anti-METTL16 or IgG1 antibody. Twenty microliters of washed Protein A Dynabeads were added to each sample for 1 hour. Beads were then washed with ice-cold RSB100-T five times and then eluted with a proteinase K solution (0.1mg/mL Proteinase K, 0.1% SDS, 20mM Tris-HCl pH 7.5, 5mM EDTA, 0.1mg/mL competitor RNA) for 30min at 37°C. Following digestion, the sa mples underwent PCA extraction and were ethanol precipitated. The resulting RNA was then used for quantitative RT-PCR.

For anti-Flag native RIP, we transfected one 10-cm plate per sample 24 hours before experiments. Media was changed to Met-free media for 2–3 hours before harvesting. Forty microliters of Anti-Flag M2 affinity gel (Sigma A2220) was used to immunoprecipitate each sample. The remaining procedure was performed as described, with volumes scaled accordingly. For the experiments in Figure S4B, Figure 6μg of Flag-tagged METTL16 (or pcDNA-FLAG) and 6ug pcDNA3 constructs were transfected. For the experiments in Figure S4F, Figure 7.5μg of FLAG-METTL16 (or pcDNA-FLAG) and 2.5μg of either β-MAT-hp1–6 A4G or β-MAT-WT were transfected as indicated. In addition, the experiments in Figure S4F omitted the MNase treatment.

M^{6}A IP and m^{6}A-seq—RNA samples were either total RNA or poly(A)-selected RNA using manufacturer's protocol of Sera-Mag Oligo (dT)-Coated Magnetic particles. In some cases, samples were RNase H treated. After precipitation, the RNA pellet was resuspended in 20μL of water, 130μL of IP Buffer (10mM Tris pH 7.5, 150mM NaCl, 0.1% Igepal), 0.5μL RNasin Plus, and 1μg of anti-m^{6}A or IgG1 antibody. Samples were nutated for 1 hour at 4°C. 15μL of washed Protein A Dynabeads were add ed to each sample and nutated for an additional hour. Beads were washed three times with IP buffer. Bound RNA was eluted by adding 200μL of G-50 buffer and 0.1mg/mL Proteinase K (Fisher Scientific) and heated to 37°C for 1 hour. Samples were then PCA extracted and ethanol precipitated.

M^{6}A-seq was performed as previously described (Dominissini et al., 2013) with the following modifications. On day 3 of knockdown in 293A–TOA cells, we added fresh media supplemented with an additional 200μM of methionine. On day 4 of knockdown, we changed to fresh media supplemented with an additional 200μM for 6 hours. After RNA

extraction, 300μg of total RNA from siCtrl or siMETTL16-1,2 treated cells was poly(A)-selected using Sera-Mag Oligo (dT)-Coated Magnetic particles. The RNA was fragmented for 5 min in fragmentation buffer and ethanol precipitated. The RNA pellet was resuspended in 100μL of water, and 5μL was removed as an “input” sample. Immunoprecipitation conditions were used as previously described, except we adjusted the total volume to 500μL. One hundred microliters of washed and pre-blocked Protein A Dynabeads were added and incubated according as previously described. Beads were washed according to Dominissini et al (2013). To elute, 250μL of G-50 buffer with 0.1mg/mL of Proteinase K was added to beads and incubated for 1 hour at 37°C. G-50 buffer was then removed to another microcentrifuge tube. Beads were washed once with an additional 250μL of G-50 buffer, and this was added to the previous elution. Samples were then PCA extracted, chloroform extracted, and ethanol precipitated. The resulting RNA constitutes the “pellet” samples. Sequencing libraries and sequencing were performed by the DNA Sequencing Center at Brigham Young University. Sequencing of the 12 samples (3 biological replicates, inputs and pellets, for siCtrl and siM16) was performed on 2 lanes an Illumina - HiSeq High-Output v4 - PE 125 Cycle with paired ends and a read length of 2 × 125 bases.

For evaluation of candidates through quantitative RT-PCR, a similar procedure was performed, though modified as specified. On day 3 of the knockdown, siRNA-treated cells were transfected with 12μg pcDNA3 or Fl-MAT2A. Six hours later, we replaced the media and supplemented with an additional 200μM of methionine. On day 4 of knockdown, we changed to fresh media supplemented with an additional 200μM for 6 hours. We used 150μg per sample and scaled the previously described m^{6}A IP procedure. Inputs and pellets were then analyzed by quantitative RT-PCR.

M^{6}A-seq Data Processing

Reads mapping and genomic coverage, gene FPKM calculation: Raw reads were aligned to the human reference genome hg38 using the bwa (v 0.7.9a–r786) aligner with default settings. Only uniquely mapped reads were kept for further analysis. For each pair, the reads were connected from the start of read1 to the end of read2 and the whole region was used for gene coverage in a strand-specific fashion. Input samples were used for calculating gene expression level (FPKM) using StringTie (v1.1.2). All the genes with average FPKM less than 1 in siCtrl sample were removed.

M^{6}A peak calling and identification of METTL16-dependent peaks: To search for enriched peaks in the m^{6}A pellet samples, we scanned each remaining gene region (including intron) using sliding windows of 100 nucleotides with 50 nucleotides overlap, and the average coverage of each window was calculated and the data were filtered at four additional steps. First, we kept windows with coverage of ≥20 in at least two of the three replicates of the m^{6}A pellet (siCtrl). For the remaining windows, for each of the three replicates we independently calculated the window coverage normalized to corresponding mean FPKM for that gene in the corresponding input samples. We then averaged the normalized values for each independent replicate to generate the average normalized values for the remaining windows for each of the four samples. These average normalized window values were the basis of all subsequent filtering steps. In the second filtering step, we

identified all potential m^6A peaks, by including only those windows that had a ratio of m^6A pellet (siCtrl) to input (siCtrl) of ≥2. Third, to select peaks that were lost upon METTL16 knockdown, we then eliminated all windows that had a ratio of m^6A pellet (siCtrl) to m^6A pellet (siM16) ≤3. Fourth, to exclude false positives that resulted low coverage in the siM16 input compared to siCtrl input, we removed windows in which input siCtrl compared to input siMETTL16 was ≥1.5. We merged the remaining windows to identify peak candidates and re-calculated the average normalized values for the merged peaks (Table S1).

Peak annotation: BedTools (v2.26) were used to get intersection of peaks and genome features. When a peak overlaps with multiple features, the feature were selected using this priority: Coding CDS exon and intron junction > Coding CDS exon > UTR3 > UTR5 > Coding intron > Noncoding exon > Noncoding_intron > Intergenic

Purification of rM16-MTD—Rosetta (DE3) cells (EMD Millipore) were transformed with SUMO-M16-MTD expression plasmid and selected in chloramphenicol and kanamycin. Colonies were inoculated into a 2mL starter culture and grown at 37°C overnight. The next day, the culture was diluted into 200mL fresh LB media with antibiotics and grown to mid-log phase (O.D.≈0.5). IPTG was added to 1mM to induce protein expression and the cultures were grown overnight at 18°C. Bacterial pe llets were harvested by centrifugation at 4000 × g for 10 min and the pellets were resuspended in 1mL lysis buffer (300mM NaCl, 50mM NaH_2PO_4, 0.5% Triton X-100, pH 8.0) supplemented with 0.5mM PMSF. Approximately 2mg lysozyme was added and the mix was incubated on ice for 30 min Subsequently, benzonase (Sigma) was added to 0.25U/uL and the mix was nutated for 30 min at room temperature. The lysate was cleared by centrifugation at 10000 × g for 30 min at 4°C and then nutated with Ni-NTA agarose bea ds (Qiagen) for 1 hr at 4°C. The beads were washed with ten column volumes of wash buffer (300mM NaCl, 50mM NaH_2PO_4, 10mM imidazole, 0.5% Triton X-100, pH 8.0) supplemented with 0.5mM PMSF. Proteins were eluted by addition of His elution buffer (300mM NaCl, 50mM NaH_2PO_4, 250mM imidazole, pH 8.0). Glycerol was added to 10% and aliquots of the protein were stored at −80°C.

***In vitro* methylation assays—**Generation of Hela nuclear extracts and methylation assays in nuclear extract were previously reported (Dignam et al., 1983; Shimba et al., 1995). Excluding contributions from nuclear extract, each 25μL methylation reaction contained 10mM HEPES (pH 7.9), 10mM $MgCl_2$, 160mM KCl, 5mM SAM (Sigma), 20μM ATP, 20U RNAsin Plus, ~10nM substrate (see below). The reactions also contained 50% nuclear extract in Buffer D (20mM HEPES [pH 7.9], 20% glycerol, 50mM KCl, 0.2mM EDTA, 0.5mM DTT). After incubation at 30°C for 1 hr, the reactions were sto pped by addition of 200μL G-50 buffer supplemented with 0.1 mg/ml Proteinase K and 15μg Glycoblue (Thermo Fisher), and incubated for an additional 30 min at 37°C. RNA was harvested by standard PCA extracti on and ethanol precipitation. RNA pellets were resuspended in 3μL of Nuclease P1 mix (30mM sodium acetate [pH 5.2], 0.33U/μL nuclease P1 [Sigma]) and incubated at 37°C for 2 hr. Digested nucleotide s were separated overnight on a cellulose thin layer chromatogroaphy (TLC) plate (Merck) in a solution of

isopropanol:HCl:H_2O (70:15:15 by volume) (Liu et al., 2013). The plate was air dried at room temperature and exposed to Phosphorimager for detection and quantification.

Immunodepletion assays were performed as described for the nuclear extract except the extract was subject to immunoprecipitation with either anti-METTL16 or anti-Flag antibodies prior to the assay. To do so, 70μL of nuclear extract plus 0.1% Igepal-CA630 was incubated with 2–3μg of antibody for 1.5 hr at 4°C while nutating. The mix was added to 20 μL of washed protein A beads (Pierce) and nutated at 4°C for an additional 1.5 hr. After careful removal from beads, the resulting supernatant was used in place of nuclear extract in a methylation reaction as described above. The beads were washed 3–5 times with Buffer D (lacking DTT) supplemented with 0.1% Igepal and resuspended in 25μL of Buffer D. This resuspended bead mix was used in place of nuclear extract in a methylation reaction as described above.

For assays with recombinant METTL16, a standard 25μL reaction contained final concentrations of 10mM HEPES (pH 7.9), 10mM $MgCl_2$, 150mM KCl, 5mM SAM, 20U RNAsin Plus, ~10nM substrate (see below), excluding contributions from 12.5μL of recombinant protein (1–5μg) in His elution buffer. Methylation of U6 substrates was significantly more salt and magnesium-sensitive than hp1 reactions. For U6 substrates, KCl and $MgCl_2$ were omitted from the reaction. Reactions were incubated at 30°C for 2 hr. The reaction was stopped as described for nuclear extracts except Proteinase K digestion was omitted. Methylation was assessed by TLC of digested nucleotides as described for the nuclear extract assays.

RNA substrates for in vitro methylation assays—Uniformly labeled substrates were generated by incorporation of α-^{32}P-ATP into standard in vitro transcription assays using PCR templates with T7 RNA polymerase promoters. To generate the PCR templates for these substrates we used primers NC2207 and NC1752 for hp1, NC2212 and NC2213 for U6, NC2317 and NC2318 for the METTL3 substrate, NC2742 and NC2743 for GNPTG, NC2744 and NC2745 for GMIP, NC2746 and NC2747 for INPPL1, NC2748 and NC2749 for PTBP1, and NC2750 and NC2751 for PP1R37 (Table S3). To make site-specific radiolabelled substrates, we performed splint ligation (Moore and Query, 2000) using synthesized RNA oligomers (Sigma) and DNA splints (Table S3). Unless otherwise specified, hp1 substrates used NC2535 as the DNA splint. U6 substrates were generated using 3-piece splint ligation. After ligation and DNase treatment, the substrates were gel purified on 6% urea-PAGE and eluted overnight in G-50 buffer. The substrates were then PCA extracted, precipitated and resuspended in water. For nuclear extract experiments, all substrates were heated to 65°C for 5 min and placed on ice immediately prior to their addition to reactions. For recombinant assays, hp1 substrates were heated to 65°C in water and slo w cooled in a heat block to ~37°C. U6 RNA substrates were heated to 65°C in 50mM NaCl and slo w cooled in a heat block to ~37°C. Of note, hp1 substrates were methylated under a variety of folding conditions, whereas U6 RNA substrates were more dependent on the specific folding conditions.

Ratio of N^6-methyladenosine to adenosine—We treated 50μg of RNA with RQ1 DNase for 1 hour at 37°C. The reaction was quenched with EDTA, then the RNA was PCA

extracted and ethanol precipitated. RNA was then resuspended in 103.5μL and digested by adding 7μL of Acidic buffer (0.1M Sodium Acetate, 20mM $ZnCl_2$ at pH 6.8), 5μg RNase A (Thermo Fisher), 3U Nuclease P1 for 4 hours at 37°C . After, 7μL of Basic Buffer (0.3M sodium acetate pH 7.8), 2U calf intestine phosphatase (New England Biolabs), and 0.0005U of Phosphodiesterase I (Sigma) were added. Reaction was incubated overnight at room temperature. Sample was then applied to an Amicon Ultra 10K MWCO column (Millipore) and centrifuged at 16000 × g for an hour. Flow through sent to mass spectrometry.

Nucleosides were detected essentially as described by Laxman et al. with minor modifications (Laxman et al., 2013). The RNA digest was first separated on a Synergi Fusion-RP column (4μm particle size, 80 Å pore size, 150 mm × 2 mm, Phenomenex) using a Shimadzu high performance liquid chromatography machine (HPLC) and simultaneously analyzed by a triple quadrupole mass spectrometer (3200 QTRAP, ABSCIEX). The total run time was 25 min at a flow rate of 0.5 ml/min, with 5mM ammonium acetate (pH 5.5) in water as Solvent A and 5mM ammonium acetate in methanol as Solvent B. The following gradient elution was performed: 0.01 min, 0% B, 4 min, 0% B, 5 min, 0.2% B, 6 min, 1% B, 7 min, 3% B, 8 min, 5% B, 14 min, 25% B, 16 min, 50% B, 18 min, 100% B, 22 min, 100% B, 23 min, 0% B, 25 min, 0% B. N6-methyladensoine and adenosine were detected by multiple reaction monitoring (MRM) using the ion pairs 282/150 and 268/136, respectively. N^6-methyladensoine was quantified using the Analyst® 1.6.1 Software package by calculating the total peak area and normalized by that of adenosine. For each experiment, authentic pure standards were injected and analyzed alongside samples.

SAM Metabolite Extraction—Procedure was adapted from published protocols (Dettmer et al., 2011)(Tu et al., 2007). In a 6-well plate, cells were washed 3 times with ice-cold PBS and 600μL of 80% methanol was added to cells. The plate was chilled on liquid N_2 for 30 seconds and moved to ice to scrape the cells. The cell/methanol solution was transferred to Eppendorf tubes and flash frozen in liquid N_2. The tubes were thawed and centrifuged at 16000 × g at 4°C for 10 min Methanol supernatant s were then transferred into new Eppendorf tubes. Cell pellets were washed with PBS, resuspended in RSB100-T and 1x SDS Buffer (2% SDS, 62.5mM Tris-HCl pH 6.8, 10% glycerol, 1% β-mercaptoethanol), and sonicated. Protein concentration was calculated to estimate cell number between samples, and methanol supernatant volumes were adjusted accordingly. A speed vacuum was used to dry pellets. Pellets were then resuspended in Solvent A (0.1% formic acid in water), centrifuged twice, and passed through a 0.2μm PVDF filter to remove insoluble particulates. Samples were analyzed using the same LC-MS/MS system as described above. The total run time was 20 min at a flow rate of 0.5 ml/min, with 0.1% formic acid in water as Solvent A and 0.1% formic acid in methanol as Solvent B. The following gradient was performed: 0.01 min, 0% B, 4 min, 0% B, 11 min, 50 % B, 13 min, 100% B, 15 min, 100% B, 16 min, 0% B, 20 min, 0% B. SAM was detected by multiple reaction monitoring (MRM) using the ion pair 399/250, quantified using the Analyst® 1.6.1 Software package by calculating the total peak area, and normalized by the total ion count (TIC). For each experiment, authentic pure SAM was injected and analyzed alongside samples.

Yeast RNA Preparation—RNA was harvested from yeast in exponential growth phase (O.D.≈0.7) using the protocol described in (Schmitt et al., 1990). Briefly, yeast were harvested by centrifugation and then resuspended in 400μL of AE buffer (50mM sodium acetate pH 5.3, 10mM EDTA). 20μL of 20% SDS was then added and the sample was vortexed. An equal volume of phenol pre-equilibrated with AE buffer was then added and mixed by vortexing. The samples were incubated at 65°C for 5min and then chilled rapidly in a dry ice-ethanol bath. Samples were then centrifuged at max speed, and the aqueous layer was transferred to a new microcentrifuge tube. The sample was then PCA extracted and ethanol precipitated.

U6 RNA immunoprecipitated nonspecficially presumably through interactions with other methylated RNAs. To reduce this background signal, we purified U6 and U2 RNAs by gel purification prior to immunoprecipitiation. To do so, 30μg of total RNA was run on a 6% Urea Gel and bands from 90–110bp and 180–200bp were excised and incubated in G-50 buffer. The RNA was then PCA extracted and ethanol precipitated. Resulting RNA was cleaved with RNase H using specified oligonucleotides (*S. pombe* U6 5', *S. pombe* U6 3', *S. pombe* U2 5') against U6 RNA or U2 RNA in order to disrupt RNA secondary structures that interfered with m^6A antibody recognition. M^6A IP was subsequently performed as described above.

Plasmids—To construct β-MAT-WT, the 3′ end of MAT2A gene was amplified using NC1145 and NC1146 (Table S3). All restriction enzymes were purchased from New England Biolabs. The PCR product was digested with EcoRI and BglII and inserted into the βΔ1(B-A) plasmid (Conrad et al., 2006) cut with the same enzymes using standard techniques. Importantly, all plasmids generated by PCR were sequence verified across the junctions and PCR insert.

The β-MAT-hp2–6m9 insert was ordered from GENEWIZ and digested with BsiWI and BglII and inserted into the β-MAT-WT cut with the same enzymes.

Deletion and mutations of MAT2A were made using SOEing PCR (Horton, 1995) with β-MAT-WT as the template, except β-MAT-hp1–6m9, which used β-MAT-hp2–6m9 as a template. In all cases, NC1576 was used as the 5′ primer and Sp6+ was used as the 3′ primer. β-MAT-Δhp1 used primers NC1653 and NC1654. β-MAT-hp1m9 used primers NC2014 and NC2015. β-MAT-hp1G3 used primers NC2137 and NC2138. β-MAT-hp1G4 used primers NC2203 and NC2204. β-MAT-hp1G4, 1xMS2 used primers NC2674 and NC2675. β-MAT-hp1U9 used primers NC2307 and NC2308. Inserts were then digested EcoRI-HF and XhoI and inserted into the β-MAT-WT cut with the same enzymes.

FL-MAT2A was generated by amplification of fully spliced MAT2A cDNA with NC1566 and NC1567. The PCR product was digested and ligated into pcDNA3-Flag cut with EcoRI and XhoI.

FLAG-tagged METTL16 was generated by amplification of fully spliced METTL16 cDNA with NC2425 and NC2426. The PCR product was digested and ligated into pcDNA3-Flag cut with BamHI-HF and XhoI. Si-resistant FLAG-METTL16 was amplified from the

previous plasmid using SOEing PCR with the previous primers and NC2521 and NC2522. Mutations of METTL16 were made with SOEing PCR with si-resistant FLAG-METTL16 as the template with the primers NC2513 and NC2514 for PP185/186AA and NC2515 and NC2156 for F187G. Inserts were then digested BamHI-HF and XhoI. MS2-METTL16 and MS2-F187G were generated by digesting either FLAG-METTL16 or FLAG-F187G with BamHI-HF and XhoI. The insert was then ligated into the pcNMS2-NLS-Flag vector cut with the same restriction enzymes. MS2-M16 MTD was generated using primers NC2425 and NC2502 with FLAG-METTL16 as the template. MS2-M16 VCR was generated using primers NC2807 and NC2426 with FLAG-METTL16 as the template. Both were digested with BamHI-HF and XhoI and then ligated into the pcNMS2-NLS-Flag vector cut with the same restriction enzymes. The NMS2-Fl-hnRNP C1 construct was generated by inserting the hnRNP C1 coding sequence amplified with NC257 and NC258 into pcNMS2 using restriction enzymes BamHI and NotI.

The rM16-MTD expression plasmid was generated by amplification of fully spliced METTL16 cDNA with NC2499 and NC2502. The PCR product was digested and ligated into pE-SUMO cut with BsaI and XbaI. The mutations of this were made by using the same primers, but amplifying from the FLAG-tagged PP185/186AA and F187G plasmids.

Quantification and Statistical Analysis

Imagequant 5.2 was used to quantify northern blots. Bands were boxed, and equal size boxes were placed along the respective columns at sites of similar background. The signal from the background box was then subtracted from the signal from the sample box to quantify real signal.

Image Studio Ver 3.1 was used to quantify western blots. Bands were selected using the “Add Rectangle” feature, and background was automatically subtracted.

Each experiment was performed with a minimal of three biological replicates and the replicate number is given in the figure legends. Mean and standard deviation were calculated as indicated. For most experiments, statistical analyses used unpaired, Student’s t-tests to test significance. For the m^{6}A-seq candidate/non-candidate experiments, p-values were determined with the Wilcoxon test. Where indicated, ns = not significant, * $p \leq 0.05$, ** $p \leq 0.01$, *** $p \leq 0.001$. In some cases, daggers (†) are used in place of asterisks to differentiate between comparisons with two different reference groups.

Data and Software Availability

The m^{6}A-seq data has been deposited to the NCBI GEO database under the accession number GSE90914.

Supplementary Material

Refer to Web version on PubMed Central for supplementary material.

Acknowledgments

We thank Drs. Joshua Mendell and John Schoggins for critical review of this manuscript, Angela Diehl for scientific illustration, and Charles Fermaintt for advice on the digitonin assays. The work was supported by the American Cancer Society RSG-14-064-01-RMC (to N.K.C.), the Cancer Prevention and Research Institute of Texas RP150596 (to Y.X.), by the National Institutes of Health R01AI123165 (to N.K.C.), R01GM094314 (to B.P.T), T32GM007062 (to K.E.P), and R01GM115473 (to Y.X.).

References

Alarcon CR, Goodarzi H, Lee H, Liu X, Tavazoie S, Tavazoie SF. HNRNPA2B1 Is a Mediator of m(6)A-Dependent Nuclear RNA Processing Events. Cell. 2015; 162:1299–1308. [PubMed: 26321680]

Amit M, Donyo M, Hollander D, Goren A, Kim E, Gelfman S, Lev-Maor G, Burstein D, Schwartz S, Postolsky B, et al. Differential GC content between exons and introns establishes distinct strategies of splice-site recognition. Cell reports. 2012; 1:543–556. [PubMed: 22832277]

Bokar JA, Shambaugh ME, Polayes D, Matera AG, Rottman FM. Purification and cDNA cloning of the AdoMet-binding subunit of the human mRNA (N6-adenosine)-methyltransferase. RNA (New York, N.Y.). 1997; 3:1233–1247.

Boutz PL, Bhutkar A, Sharp PA. Detained introns are a novel, widespread class of post-transcriptionally spliced introns. Genes Dev. 2015; 29:63–80. [PubMed: 25561496]

Braunschweig U, Barbosa-Morais NL, Pan Q, Nachman EN, Alipanahi B, Gonatopoulos-Pournatzis T, Frey B, Irimia M, Blencowe BJ. Widespread intron retention in mammals functionally tunes transcriptomes. Genome Res. 2014; 24:1774–1786. [PubMed: 25258385]

Bresson SM, Hunter OV, Hunter AC, Conrad NK. Canonical Poly(A) Polymerase Activity Promotes the Decay of a Wide Variety of Mammalian Nuclear RNAs. PLoS Genet. 2015; 11:e1005610. [PubMed: 26484760]

Brow DA, Guthrie C. Spliceosomal RNA U6 is remarkably conserved from yeast to mammals. Nature. 1988; 334:213–218. [PubMed: 3041282]

Brown JA, Kinzig CG, DeGregorio SJ, Steitz JA. Methyltransferase-like protein 16 binds the 3'-terminal triple helix of MALAT1 long noncoding RNA. Proc. Natl. Acad. Sci. U. S. A. 2016; 113:14013–14018. [PubMed: 27872311]

Conrad NK. Chapter 15. Co-immunoprecipitation techniques for assessing RNA-protein interactions in vivo. Methods Enzymol. 2008; 449:317–342. [PubMed: 19215765]

Conrad NK, Mili S, Marshall EL, Shu MD, Steitz JA. Identification of a rapid mammalian deadenylation-dependent decay pathway and its inhibition by a viral RNA element. Mol. Cell. 2006; 24:943–953. [PubMed: 17189195]

Conrad NK, Steitz JA. A Kaposi's sarcoma virus RNA element that increases the nuclear abundance of intronless transcripts. The EMBO journal. 2005; 24:1831–1841. [PubMed: 15861127]

Coulter AW, Lombardini JB, Sufrin JR, Talalay P. Structural and conformational analogues of L-methionine as inhibitors of the enzymatic synthesis of S-adenosyl-l-methionine. 3. Carbocyclic and heterocyclic amino acids. Mol. Pharmacol. 1974; 10:319–334. [PubMed: 4859493]

Dettmer K, Nurnberger N, Kaspar H, Gruber MA, Almstetter MF, Oefner PJ. Metabolite extraction from adherently growing mammalian cells for metabolomics studies: optimization of harvesting and extraction protocols. Anal. Bioanal. Chem. 2011; 399:1127–1139. [PubMed: 21125262]

Dignam JD, Lebovitz RM, Roeder RG. Accurate transcription initiation by RNA polymerase II in a soluble extract from isolated mammalian nuclei. Nucleic Acids Res. 1983; 11:1475–1489. [PubMed: 6828386]

Dominissini D, Moshitch-Moshkovitz S, Salmon-Divon M, Amariglio N, Rechavi G. Transcriptome-wide mapping of N(6)-methyladenosine by m(6)A-seq based on immunocapturing and massively parallel sequencing. Nat. Protoc. 2013; 8:176–189. [PubMed: 23288318]

Dominissini D, Moshitch-Moshkovitz S, Schwartz S, Salmon-Divon M, Ungar L, Osenberg S, Cesarkas K, Jacob-Hirsch J, Amariglio N, Kupiec M, et al. Topology of the human and mouse m6A RNA methylomes revealed by m6A–seq. Nature. 2012; 485:201–206. [PubMed: 22575960]

Dorsett M, Westlund B, Schedl T. METT-10, a putative methyltransferase, inhibits germ cell proliferative fate in Caenorhabditis elegans. Genetics. 2009; 183:233–247. [PubMed: 19596901]

Du H, Zhao Y, He J, Zhang Y, Xi H, Liu M, Ma J, Wu L. YTHDF2 destabilizes m(6)A-containing RNA through direct recruitment of the CCR4-NOT deadenylase complex. Nature communications. 2016; 7:12626.

Epstein P, Reddy R, Henning D, Busch H. The nucleotide sequence of nuclear U6 (4.7 S) RNA. J. Biol. Chem. 1980; 255:8901–8906. [PubMed: 6773955]

Gu J, Patton JR, Shimba S, Reddy R. Localization of modified nucleotides in Schizosaccharomyces pombe spliceosomal small nuclear RNAs: modified nucleotides are clustered in functionally important regions. RNA (New York, N.Y.). 1996; 2:909–918.

Halim AB, LeGros L, Geller A, Kotb M. Expression and functional interaction of the catalytic and regulatory subunits of human methionine adenosyltransferase in mammalian cells. J. Biol. Chem. 1999; 274:29720–29725. [PubMed: 10514445]

Harada F, Kato N, Nishimura S. The nucleotide sequence of nuclear 4.8S RNA of mouse cells. Biochem. Biophys. Res. Commun. 1980; 95:1332–1340. [PubMed: 6251836]

Horton RM. PCR-mediated recombination and mutagenesis. SOEing together tailor-made genes. Mol. Biotechnol. 1995; 3:93–99. [PubMed: 7620981]

Ke S, Alemu EA, Mertens C, Gantman EC, Fak JJ, Mele A, Haripal B, Zucker-Scharff I, Moore MJ, Park CY, et al. A majority of m6A residues are in the last exons, allowing the potential for 3' UTR regulation. Genes Dev. 2015; 29:2037–2053. [PubMed: 26404942]

Kim J, Kim Y, Yeom M, Kim JH, Nam HG. FIONA1 is essential for regulating period length in the Arabidopsis circadian clock. The Plant cell. 2008; 20:307–319. [PubMed: 18281507]

Laxman S, Sutter BM, Wu X, Kumar S, Guo X, Trudgian DC, Mirzaei H, Tu BP. Sulfur amino acids regulate translational capacity and metabolic homeostasis through modulation of tRNA thiolation. Cell. 2013; 154:416–429. [PubMed: 23870129]

Li H, Durbin R. Fast and accurate short read alignment with Burrows-Wheeler transform. Bioinformatics (Oxford, England). 2009; 25:1754–1760.

Lin S, Choe J, Du P, Triboulet R, Gregory RI. The m(6)A Methyltransferase METTL3 Promotes Translation in Human Cancer Cells. Mol. Cell. 2016; 62:335–345.

Linder B, Grozhik AV, Olarerin-George AO, Meydan C, Mason CE, Jaffrey SR. Single-nucleotide-resolution mapping of m6A and m6Am throughout the transcriptome. Nat. Methods. 2015; 12:767–772. [PubMed: 26121403]

Liu J, Yue Y, Han D, Wang X, Fu Y, Zhang L, Jia G, Yu M, Lu Z, Deng X, et al. A METTL3-METTL14 complex mediates mammalian nuclear RNA N6-adenosine methylation. Nat. Chem. Biol. 2014; 10:93–95. [PubMed: 24316715]

Liu N, Dai Q, Zheng G, He C, Parisien M, Pan T. N(6)-methyladenosine-dependent RNA structural switches regulate RNA-protein interactions. Nature. 2015; 518:560–564. [PubMed: 25719671]

Liu N, Parisien M, Dai Q, Zheng G, He C, Pan T. Probing N6-methyladenosine RNA modification status at single nucleotide resolution in mRNA and long noncoding RNA. RNA (New York, N.Y.). 2013; 19:1848–1856.

Luo S, Tong L. Molecular basis for the recognition of methylated adenines in RNA by the eukaryotic YTH domain. Proc. Natl. Acad. Sci. U. S. A. 2014; 111:13834–13839. [PubMed: 25201973]

Lykke-Andersen J, Shu MD, Steitz JA. Communication of the position of exon-exon junctions to the mRNA surveillance machinery by the protein RNPS1. Science (New York, N.Y.). 2001; 293:1836–1839.

Malone T, Blumenthal RM, Cheng X. Structure-guided analysis reveals nine sequence motifs conserved among DNA amino-methyltransferases, and suggests a catalytic mechanism for these enzymes. J. Mol. Biol. 1995; 253:618–632. [PubMed: 7473738]

Martinez-Chantar ML, Latasa MU, Varela-Rey M, Lu SC, Garcia-Trevijano ER, Mato JM, Avila MA. L-methionine availability regulates expression of the methionine adenosyltransferase 2A gene in human hepatocarcinoma cells: role of S-adenosylmethionine. J. Biol. Chem. 2003; 278:19885–19890. [PubMed: 12660248]

Meyer KD, Patil DP, Zhou J, Zinoviev A, Skabkin MA, Elemento O, Pestova TV, Qian SB, Jaffrey SR. 5' UTR m(6)A Promotes Cap-Independent Translation. Cell. 2015; 163:999–1010. [PubMed: 26593424]

Meyer KD, Saletore Y, Zumbo P, Elemento O, Mason CE, Jaffrey SR. Comprehensive analysis of mRNA methylation reveals enrichment in 3' UTRs and near stop codons. Cell. 2012; 149:1635–1646. [PubMed: 22608085]

Moore MJ, Query CC. Joining of RNAs by splinted ligation. Methods Enzymol. 2000; 317:109–123. [PubMed: 10829275]

Mougin A, Gottschalk A, Fabrizio P, Luhrmann R, Branlant C. Direct probing of RNA structure and RNA-protein interactions in purified HeLa cell's and yeast spliceosomal U4/U6.U5 tri-snRNP particles. J. Mol. Biol. 2002; 317:631–649. [PubMed: 11955014]

Nguyen TH, Galej WP, Fica SM, Lin PC, Newman AJ, Nagai K. CryoEM structures of two spliceosomal complexes: starter and dessert at the spliceosome feast. Curr. Opin. Struct. Biol. 2016; 36:48–57. [PubMed: 26803803]

Orzalli MH, Broekema NM, Diner BA, Hancks DC, Elde NC, Cristea IM, Knipe DM. cGAS-mediated stabilization of IFI16 promotes innate signaling during herpes simplex virus infection. Proc. Natl. Acad. Sci. U. S. A. 2015; 112:E1773–1781. [PubMed: 25831530]

Parker BJ, Moltke I, Roth A, Washietl S, Wen J, Kellis M, Breaker R, Pedersen JS. New families of human regulatory RNA structures identified by comparative analysis of vertebrate genomes. Genome Res. 2011; 21:1929–1943. [PubMed: 21994249]

Patil DP, Chen CK, Pickering BF, Chow A, Jackson C, Guttman M, Jaffrey SR. m6A RNA methylation promotes XIST-mediated transcriptional repression. Nature. 2016; 537:369–373. [PubMed: 27602518]

Pertea M, Pertea GM, Antonescu CM, Chang TC, Mendell JT, Salzberg SL. StringTie enables improved reconstruction of a transcriptome from RNA-seq reads. Nat. Biotechnol. 2015; 33:290–295. [PubMed: 25690850]

Ping XL, Sun BF, Wang L, Xiao W, Yang X, Wang WJ, Adhikari S, Shi Y, Lv Y, Chen YS, et al. Mammalian WTAP is a regulatory subunit of the RNA N6-methyladenosine methyltransferase. Cell Res. 2014; 24:177–189. [PubMed: 24407421]

Quinlan AR, Hall IM. BEDTools: a flexible suite of utilities for comparing genomic features. Bioinformatics (Oxford, England). 2010; 26:841–842.

Ran FA, Hsu PD, Wright J, Agarwala V, Scott DA, Zhang F. Genome engineering using the CRISPR-Cas9 system. Nat. Protoc. 2013; 8:2281–2308. [PubMed: 24157548]

Sahin BB, Patel D, Conrad NK. Kaposi's sarcoma-associated herpesvirus ORF57 protein binds and protects a nuclear noncoding RNA from cellular RNA decay pathways. PLoS Path. 2010; 6:e1000799.

Schmitt ME, Brown TA, Trumpower BL. A rapid and simple method for preparation of RNA from Saccharomyces cerevisiae. Nucleic Acids Res. 1990; 18:3091–3092. [PubMed: 2190191]

Schwartz S, Mumbach MR, Jovanovic M, Wang T, Maciag K, Bushkin GG, Mertins P, Ter-Ovanesyan D, Habib N, Cacchiarelli D, et al. Perturbation of m6A writers reveals two distinct classes of mRNA methylation at internal and 5' sites. Cell reports. 2014; 8:284–296. [PubMed: 24981863]

Sergiev PV, Serebryakova MV, Bogdanov AA, Dontsova OA. The ybiN gene of Escherichia coli encodes adenine-N6 methyltransferase specific for modification of A1618 of 23 S ribosomal RNA, a methylated residue located close to the ribosomal exit tunnel. J. Mol. Biol. 2008; 375:291–300. [PubMed: 18021804]

Shimba S, Bokar JA, Rottman F, Reddy R. Accurate and efficient N-6-adenosine methylation in spliceosomal U6 small nuclear RNA by HeLa cell extract in vitro. Nucleic Acids Res. 1995; 23:2421–2426. [PubMed: 7630720]

Sledz P, Jinek M. Structural insights into the molecular mechanism of the m(6)A writer complex. eLife. 2016:5.

Tu BP, Mohler RE, Liu JC, Dombek KM, Young ET, Synovec RE, McKnight SL. Cyclic changes in metabolic state during the life of a yeast cell. Proc. Natl. Acad. Sci. U. S. A. 2007; 104:16886–16891. [PubMed: 17940006]

Wang JX, Breaker RR. Riboswitches that sense S-adenosylmethionine and S-adenosylhomocysteine. Biochemistry and cell biology = Biochimie et biologie cellulaire. 2008; 86:157–168. [PubMed: 18443629]

Wang P, Doxtader KA, Nam Y. Structural Basis for Cooperative Function of Mettl3 and Mettl14 Methyltransferases. Mol. Cell. 2016a; 63:306–317.

Wang T, Birsoy K, Hughes NW, Krupczak KM, Post Y, Wei JJ, Lander ES, Sabatini DM. Identification and characterization of essential genes in the human genome. Science (New York, N.Y.). 2015; 350:1096–1101.

Wang X, Feng J, Xue Y, Guan Z, Zhang D, Liu Z, Gong Z, Wang Q, Huang J, Tang C, et al. Structural basis of N(6)-adenosine methylation by the METTL3-METTL14 complex. Nature. 2016b; 534:575–578. [PubMed: 27281194]

Wang X, Lu Z, Gomez A, Hon GC, Yue Y, Han D, Fu Y, Parisien M, Dai Q, Jia G, et al. N6-methyladenosine-dependent regulation of messenger RNA stability. Nature. 2014; 505:117–120. [PubMed: 24284625]

Xiao W, Adhikari S, Dahal U, Chen YS, Hao YJ, Sun BF, Sun HY, Li A, Ping XL, Lai WY, et al. Nuclear m(6)A Reader YTHDC1 Regulates mRNA Splicing. Mol. Cell. 2016; 61:507–519. [PubMed: 26876937]

Yap K, Lim ZQ, Khandelia P, Friedman B, Makeyev EV. Coordinated regulation of neuronal mRNA steady-state levels through developmentally controlled intron retention. Genes Dev. 2012; 26:1209–1223. [PubMed: 22661231]

Yue Y, Liu J, He C. RNA N6-methyladenosine methylation in post-transcriptional gene expression regulation. Genes Dev. 2015; 29:1343–1355. [PubMed: 26159994]

Zhou J, Wan J, Gao X, Zhang X, Jaffrey SR, Qian SB. Dynamic m(6)A mRNA methylation directs translational control of heat shock response. Nature. 2015; 526:591–594. [PubMed: 26458103]

Highlights

- Intron retention of the SAM synthetase MAT2A RNA is responsive to SAM levels
- METTL16 and a conserved hairpin (hp1) are required for induction of MAT2A splicing
- Occupancy of METTL16 on hp1 promotes splicing of the MAT2A retained intron
- METTL16 m^6A methylates MAT2A hairpins and the spliceosomal U6 snRNA

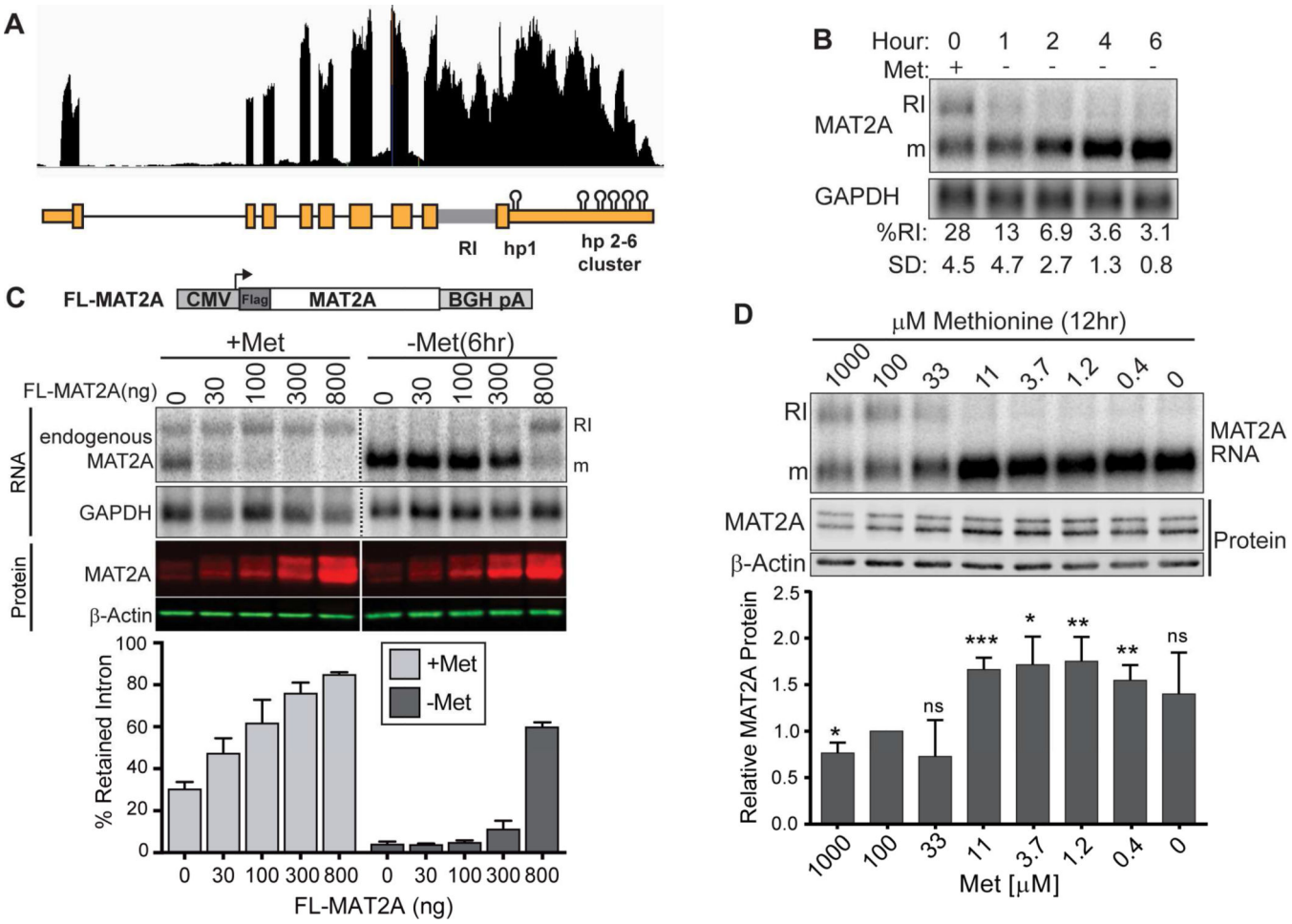

Figure 1. MAT2A Intron Retention Is Regulated

(A) RNA-seq trace of MAT2A from poly(A)-selected total RNA. The retained intron (RI) is highlighted in gray. (B) MAT2A northern blot from Met depletion time course. Data are mean ± standard deviation (SD); n=3. GAPDH serves as loading control. RI and m are MAT2A–RI and mRNA isoforms, respectively. (C) *Top*, Endogenous MAT2A and GAPDH northern blots with RNA from MAT2A overexpressing cells. Intervening lanes were removed (dashed lines), but the same exposure is shown. *Middle*, Western blot of MAT2A. The antibody recognizes both endogenous and overexpressed MAT2A. The doublet reflects two posttranslationally modified protein isoforms (α2 and α2′)(Halim et al., 1999). *Bottom*, quantification of the northern blots; data are mean ± SD; n=3. (D) Northern and western blot analyses after a 12-hr shift to the indicated Met concentrations. Protein is quantified below as mean ± SD; n=3. Unless otherwise noted, all statistical analyses are unpaired Student's *t*-tests and significance is annotated as not significant (ns), $p \leq 0.05$ (*), $p \leq 0.01$ (**), or $p \leq 0.001$ (***). Here, comparisons were made to the 100 μM sample. See also Figure S1.

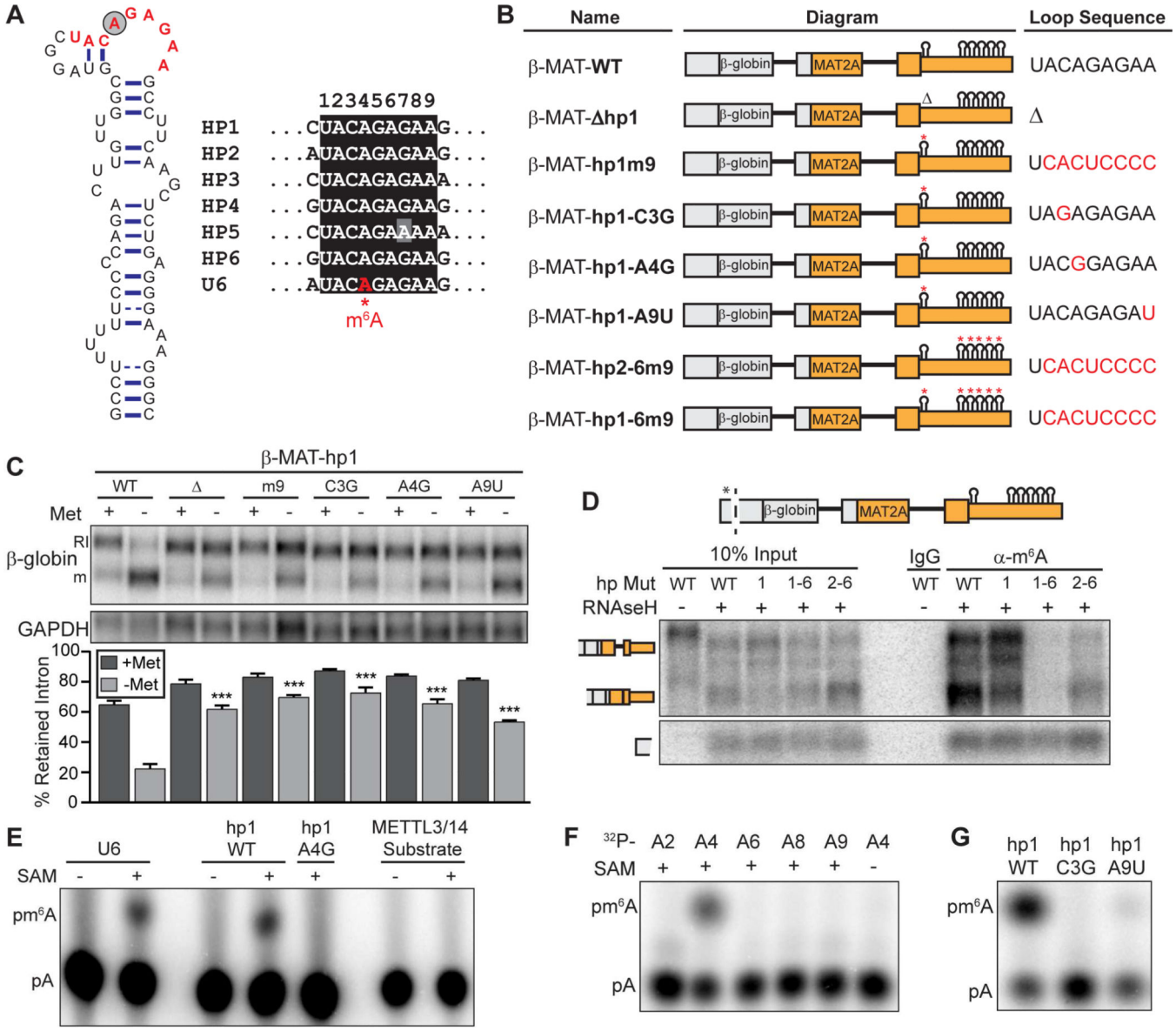

Figure 2. MAT2A Hairpin 1 Is Necessary for Regulation of Intron Retention and Has an N^6-Methyladenosine Modification

(A) *Left*, Structure of MAT2A hp1. Red, conserved nonamer; gray circle, predicted m^{6}A (A4). *Right*, Alignment of MAT2A conserved nonamers and U6 snRNA m^{6}A site. (B) Diagram of β-globin-MAT2A reporters. Red asterisks, mutation sites. (C) Northern blot and quantification of β-globin reporter assay. Data are mean ± SD; n=4. Statistical analysis compared all –Met samples to the WT-Met control (lane 2). (D) M^{6}A-IP experiment with indicated β-globin reporters. RNase H cleavage site is shown as dashed lines; all hp mutants are m9 (see panel B). (E) TLC from an *in vitro* methylation assay in nuclear extract with uniformly labeled substrates. (F) Same as (E) except the hp1 RNA substrates were radiolabeled at specific adenosines. (G) Same as (F) with A4-labeled WT, C3G, or A9U substrates. See also Figure S2.

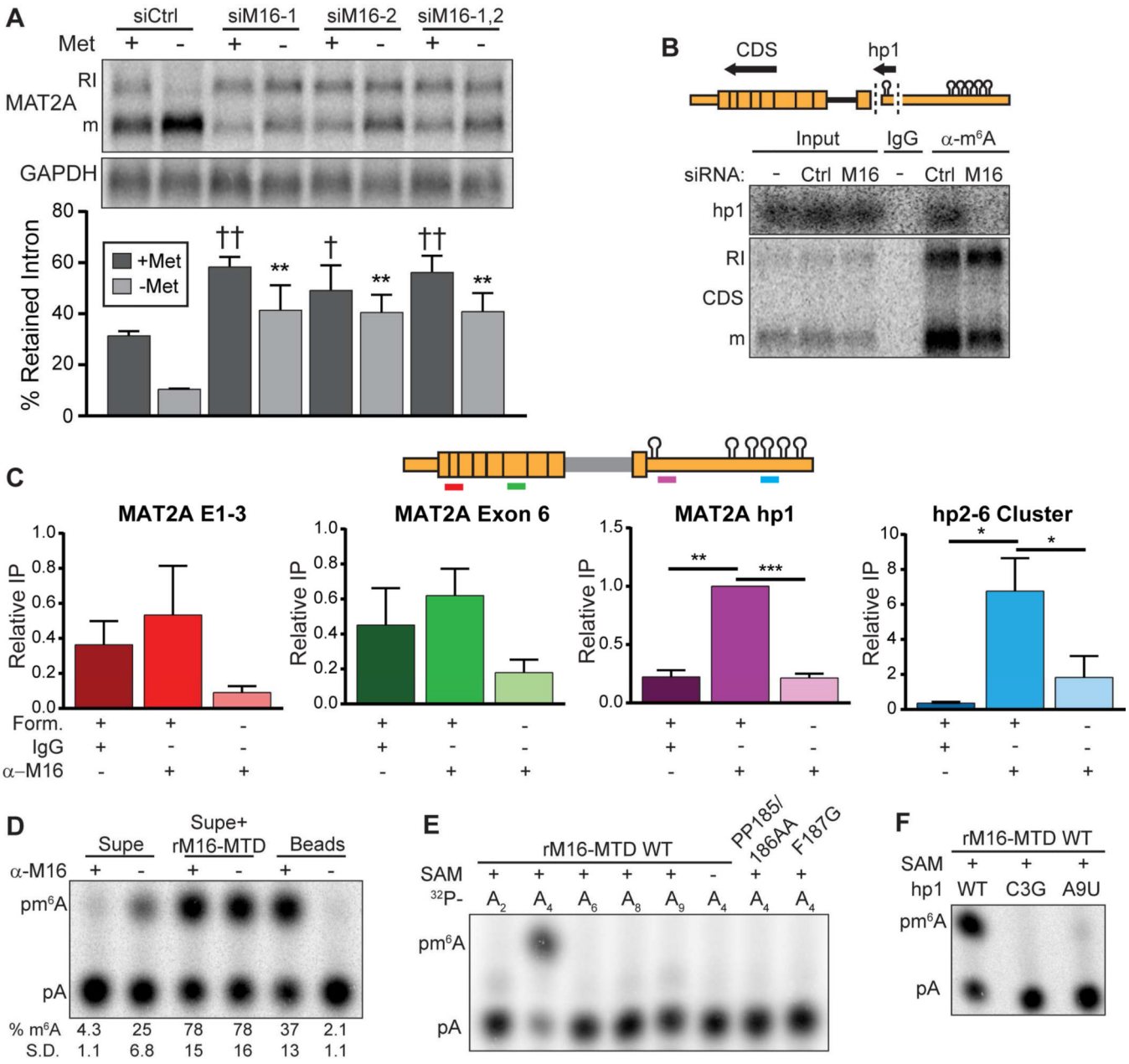

Figure 3. METTL16 Methylates the MAT2A Hairpins and Is Required for Splicing Induction

(A) Northern blot of MAT2A after knockdown with control siRNAs (siCtrl), or two METTL16 siRNAs transfected individually or together. Met was depleted for 4 hours. Quantification is mean ± SD; n=4. Statistical analysis compared –Met samples to siCtrl–Met (asterisks), and +Met samples to siCtrl+Met (daggers). (B) *Top*, Schematic of the MAT2A probes (arrows) and sites of RNase H cleavage (dashed lines). *Bottom*, Northern blot of m^{6}A-IP with poly(A)-selected, RNase H-treated RNA from cells after the indicated siRNA treatments. (C) Formaldehyde RIP of METTL16 with MAT2A RNA. RT-qPCR amplicons are shown; the anti-M16/+Form value for hp1 was set to 1. Data are mean ± SD; n=3. (D) TLC from METTL16 immunodepletion experiment using hp1 radiolabeled at position A4 as substrate. Data are mean ± SD; n=3. (E) *In vitro* methylation assay using wild-type or

mutant rM16-MTD with site-specific radiolabeled hp1 substrates. (F) *In vitro* methylation assay using wild-type rM16-MTD with A4-labeled WT or mutant substrates. See also Figure S3.

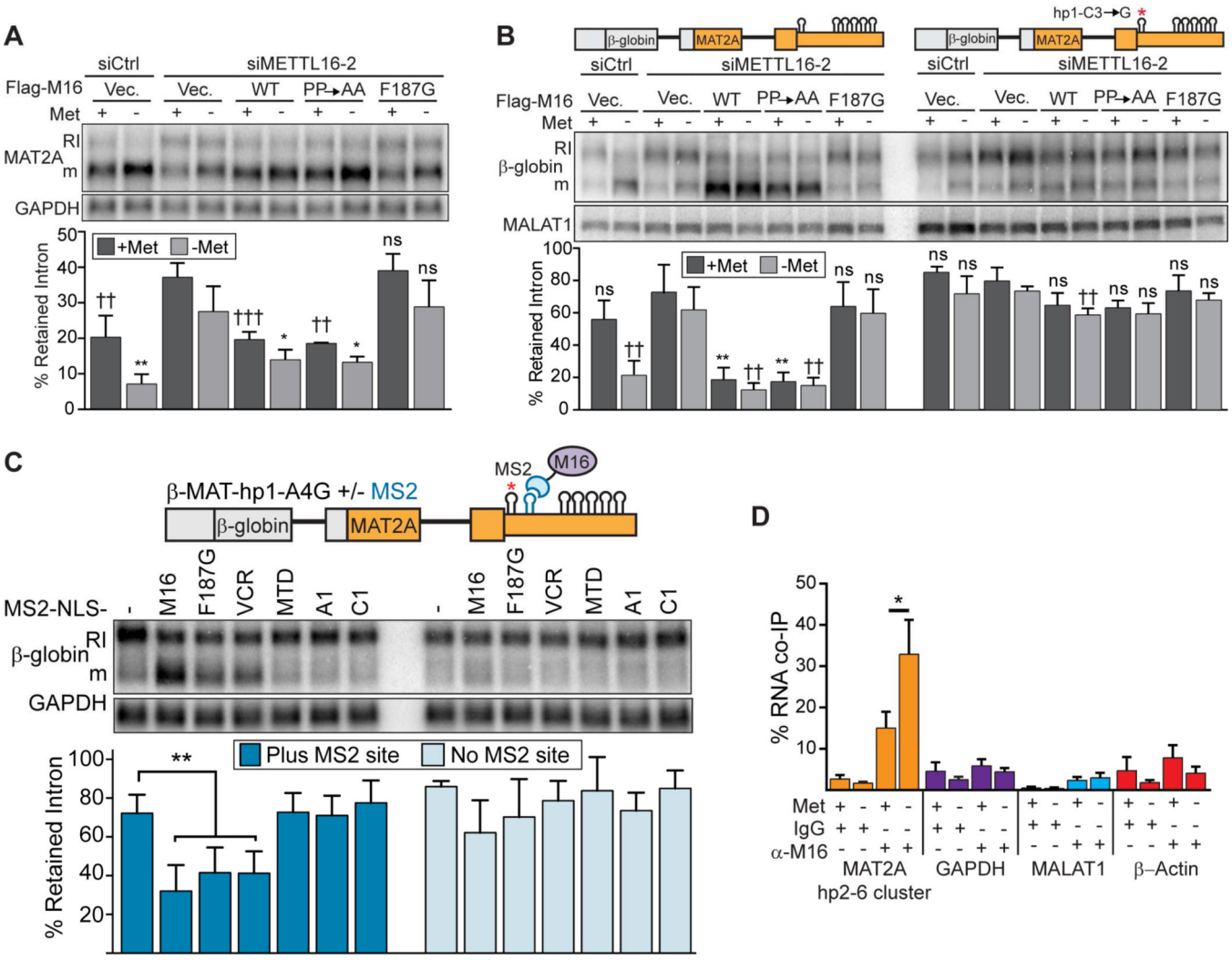

Figure 4. METTL16 Dwell Time on Hairpin 1 Regulates MAT2A Intron Retention

(A) Northern blot of MAT2A after knockdown of METTL16 and overexpression with Flag-tagged siRNA resistant METTL16 proteins (Vec., empty vector; WT, FLAG-METTL16; PP→AA, FLAG-PP185/186AA; F187G, FLAG-F187G). Data are mean ± SD; *n*=4. Statistical analysis compared all –Met samples to - Met/vector (asterisks), and all +Met samples to +Met/vector (daggers). (B) Same as (A) except β-globin reporters, β-MAT-WT or β-MAT-hp1-C3G, were assayed. Data represented as mean ± SD; *n*≥3. (C) Diagram of MS2 tethering strategy, representative northern blot, and quantification of intron retention (dark blue, with MS2 binding sites; light blue, no MS2 binding site). The MS2 fusions include a nuclear localization signal (NLS). Data are mean ± SD; *n*=4. (D) METTL16 native RIP with extracts from cells grown for 3 hr +/−Met. Limited RNA digestion was performed and the MALAT1 amplicon is over 5 kb from the METTL16 binding site, so it serves as a negative control along with GAPDH and β-actin (Brown et al., 2016). Data are mean ± SD; *n*=3. See also Figure S4.

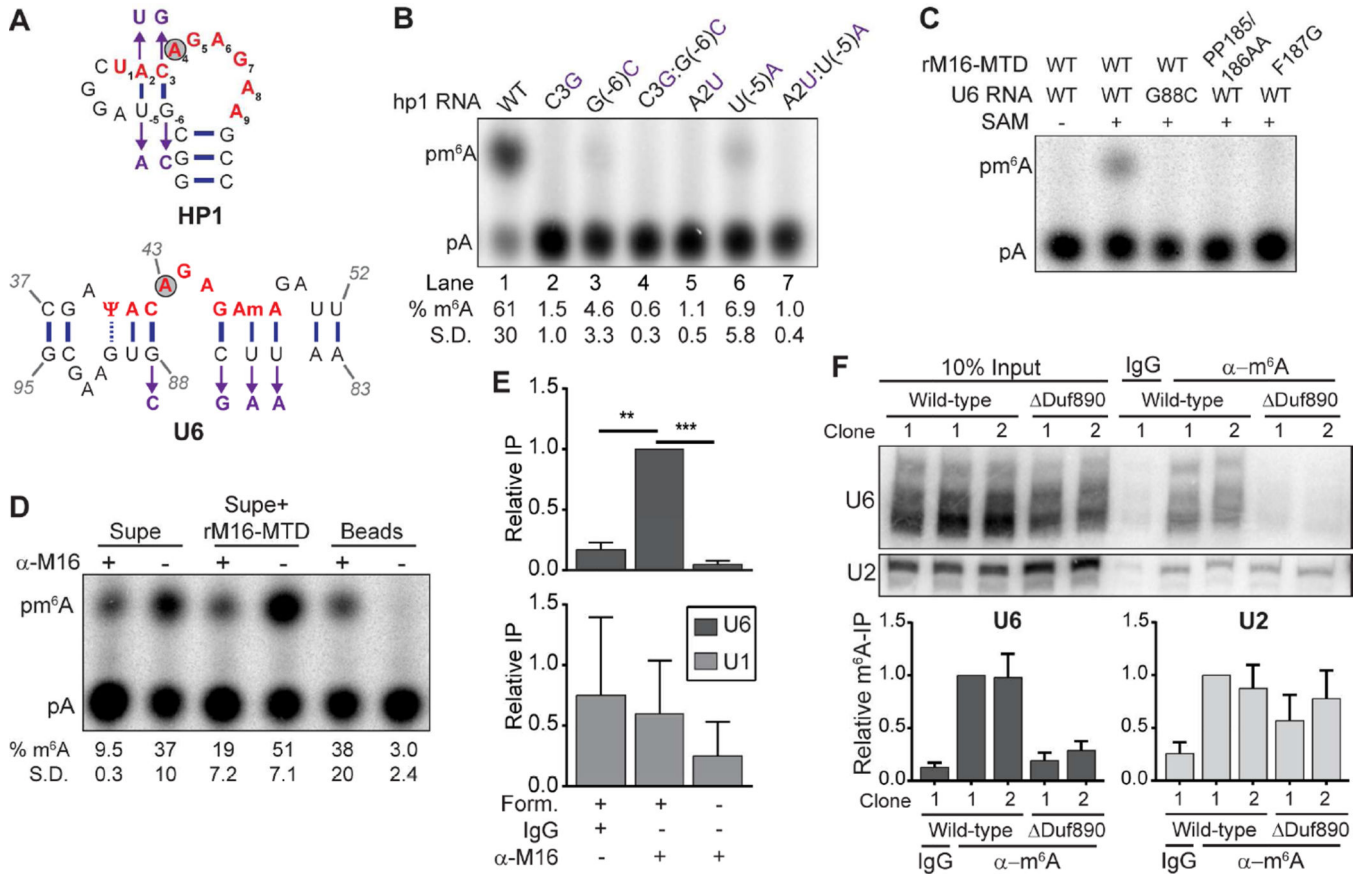

Figure 5. METTL16 Is the U6 snRNA N^6-Methyltranfserase

(A) Predicted structures surrounding the MAT2A hp1 and U6 snRNA methylation sites (gray circles). Red, conserved nonamer; Purple, mutants. (B) *In vitro* methylation with rM16-MTD and indicated hp1 substrates. Data are mean ± SD; n=3. (C) *In vitro* methylation assay using a site-specifically radiolabeled full-length WT or G88C U6 RNA substrates with rM16-MTD, PP185/186AA, or F187G. (D) Immunodepletion assay (Figure 3D) using a U6 snRNA substrate. Quantification is mean ± SD; n=3. (E) Formaldehyde RIP of METTL16 with U6 and U1 snRNAs. The anti-M16/+Form for U6 was set to 1. Data are mean ± SD; n=3. (F) M^{6}A-IP of RNA from two independent colonies of wild-type or ΔDuf890 *S. pombe* strains. The IP efficiency for the wild-type clone 1 was set to 1. Data are mean ± SD; n=5. See also Figure S5.

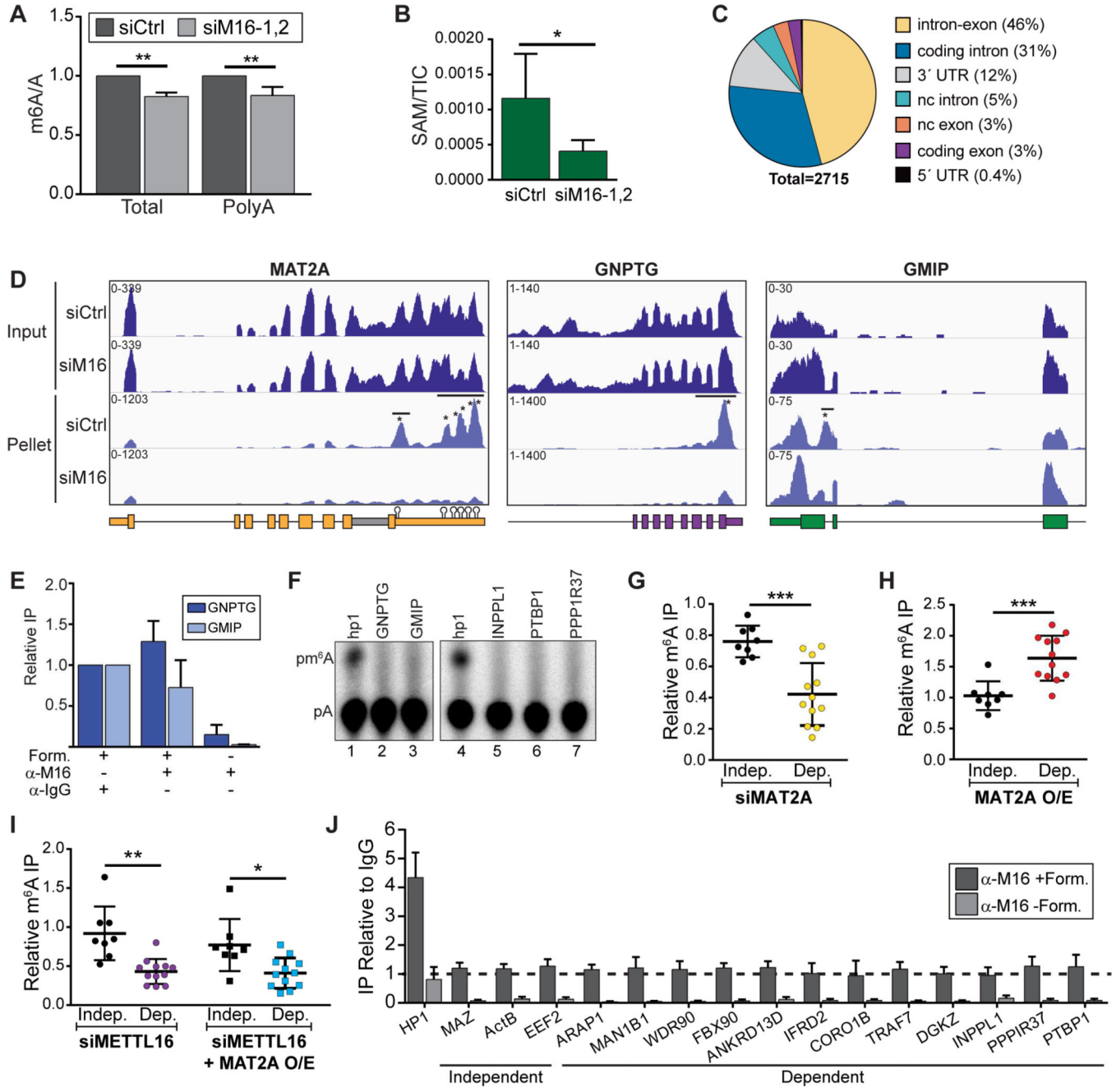

Figure 6. Global Analysis of M^{6}A After METTL16 Knockdown

(A) Ratio of m^{6}A to A in total and poly(A)-selected RNA after METTL16 knockdown; siCtrl was set to 1. Data are mean ± SD; n≥4. (B) Intracellular SAM levels normalized to total ion count (TIC) after METTL16 knockdown. Data are mean ± SD; n=6. (C) Pie chart depicting the annotations of the m^{6}A peaks that decrease upon METTL16 knockdown. (D) RNA-seq traces from the m^{6}A-seq. The peaks and UACAGAGAA sites are indicated by bars and asterisks, respectively. (E) Formaldehyde RIP as in Figure 3C; the IgG control was set to 1. Data are mean ± SD; n=3. (F) *In vitro* methylation assay as in Figure 2E. (G) M^{6}A-IP was performed on RNA from cells in which MAT2A was knocked down. The m^{6}A-IP efficiency

was compared to siCtrl samples for a panel of twelve METTL16-dependent and nine METTL16-independent m^6A peaks (Figure S5E). Each point is the average m^6A-IP efficiency for a specific peak. (H) Same as (G) except MAT2A was overexpressed. (I) Same as (G) except RNA from siM16-treated cells was assessed +/−MAT2A overexpression. (J) Formaldehyde RIP as in (E). The IP efficiency of the IgG control was set to one, but is not shown. See also Figure S5.

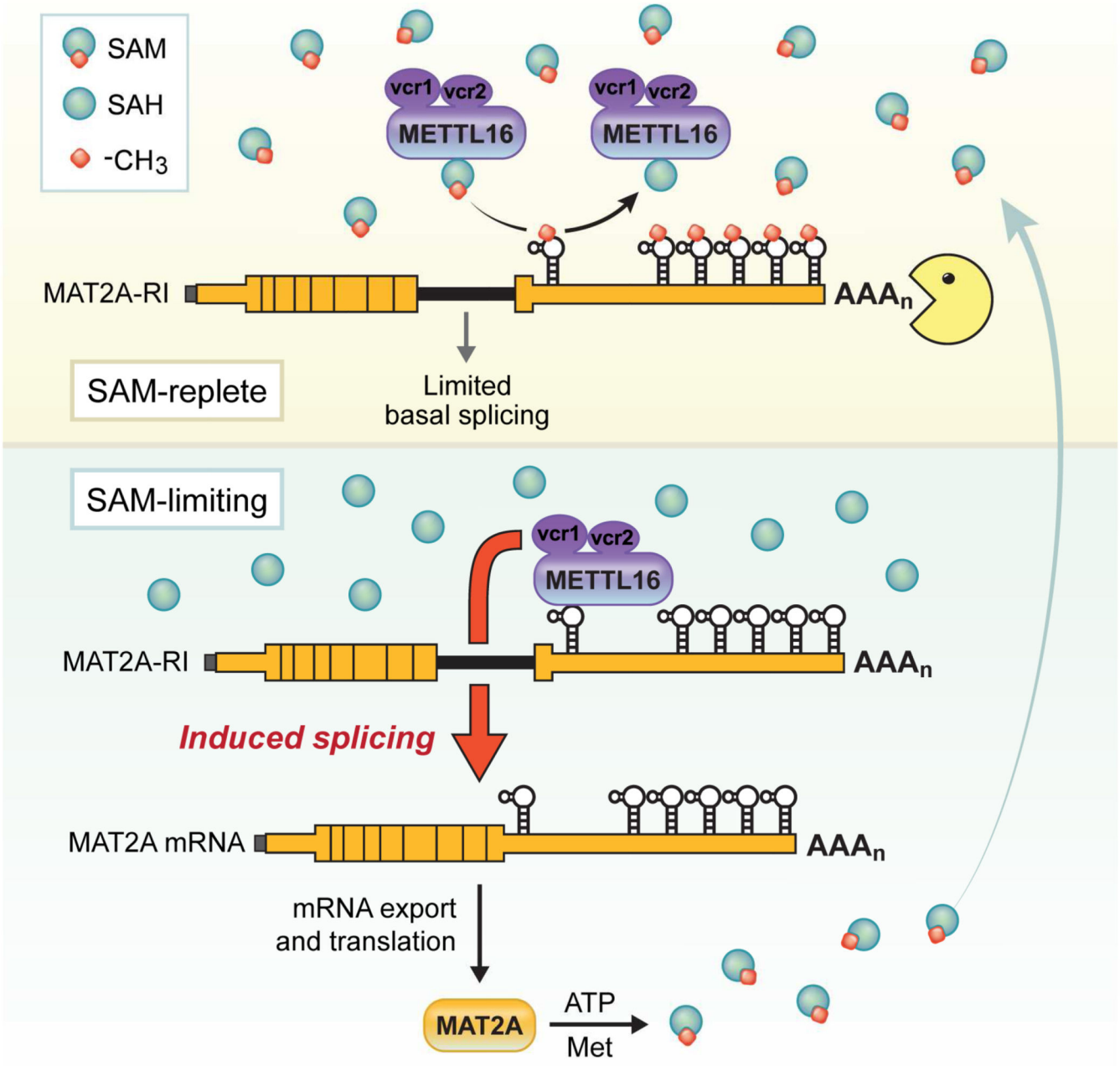

Figure 7. Model For METTL16 Activation Of MAT2A Splicing In Response To SAM Levels

We propose that SAM abundance controls the dwell-time of METTL16 on the MAT2A hp1 by modulating its methylation efficiency. In turn, METTL16 occupancy promotes efficient splicing. See text for details. The diagram depicts posttranscriptional splicing induction, but our data are also consistent with METTL16 promoting co-transcriptional splicing.